(2)

FINAL TECHNICAL REPORT
TO
THE OFFICE OF NAVAL RESEARCH
GRANT #N00014-89-J-1779

The Magnetochemistry of Supramolecular Particles: The Transition from the Molecular to the Solid-State

Principal Investigator

Georgia C. Papaefthymiou
Francis Bitter National Magnet Laboratory
Massachusetts Institute of Technology
Cambridge, MA 02139

May, 1992

CONTENTS

Abstract

The magnetic properties of nanometer-sized molecular complexes or clusters that contain an increasing number n of superexchange-coupled iron ions ($10 \leq n \leq 20$) participating in 3-D or lower-dimensional magnetic interactions were examined. The experimental criteria that establish the onset of incipient solid-state magnetic correlation effects in these molecules were emphasized. These chemical structures are beyond the molecular realm but convergence to the bulk has not yet been attained. Thus, they afforded appropriate experimental systems to test theoretical predictions that the onset of incipient solid-state phenomena — such as the emergence of a conduction band in metallic clusters and collective magnetic interactions responsible for magnetic ordering in solids — occurs at the vicinity of $n \geq 10$, where n is the number of atoms or interacting spins in the cluster.

The study provided, by means of Mössbauer spectroscopy with a characteristic measuring time $\tau_m \sim 10^{-8}$ sec, the first experimental observation of the onset of intramolecular magnetic ordering in 10 Å diameter clusters whose magnetic exchange interaction network among iron ions was three-dimensional. Owing to the extremely small size of the magnetic domain transitional magnetic behavior and superparamagnetic relaxation phenomena dominated the Mössbauer spectra. In addition, preliminary magnetization studies on a mixed valent cluster containing iron ions primarily in the ferrous state indicate the presence of hysteretic effects at low temperatures, which also attests to the existence of collective magnetic interactions and particle-like magnetic behavior of these macromolecules. This is the first time that hysteresis has been observed in nanometer-sized molecular systems. Due to spin fluctuation effects lower dimensional clusters failed to produce collective magnetic correlation phenomena within the Mössbauer time window down to pumped liquid helium temperatures.

Summary

Controlled polymerization of iron in nonaqueous solvents leads to the synthesis of molecular clusters of ever-increasing size, tending to extended structures. Polymerization of oxo-bridged octahedrally coordinated iron has produced one nanometer-sized clusters with 3D and lower magnetic dimensionality, while sulfide- and selenide-bridged tetrahedrally coordinated iron ions have yielded molecular clusters of lower magnetic dimensionality. The electronic and magnetic properties of these clusters were investigated in order to determine the presence of extended electronic states and the onset of collective magnetic correlations associated with the solid state.

In all, eight clusters were examined of iron nuclearity Fe_{10}, Fe_{11}, Fe_{12}, Fe_{16}, Fe_{17}, Fe_{18}, and Fe_{20}, with the following stoichiometries:

$[Fe(OCH_3)_2(O_2CCH_2Cl)]_{10}$ (1)

$[Fe_{11}O_6(OH)_6(O_2CPh)_{15}] \cdot 6THF$ (2)

$[Fe_{12}(O)_2(OCH_3)_{14}(O_3CCH_3)_{10}(CH_3OH)_2]Li_2$ (3)

$[Fe_{12}(O)_2(OCH_3)_{18}(O_2CCH_3)_6(CH_3OH)_4]$ (4)

$[Fe_{16}MnO_{10}(OH)_{10}(CO_2CPh)_{20}]$ (5)

$[Fe_{17}O_{10}(OH)_{10}(O_2CPh)_{20}]$ (6)

$(Pr_4N)_6Na_4Fe_{18}S_{30} \cdot 14MeCN$ (7)

$(Bu_4N)_{4.5}\ Na_{13.5}Fe_{20}Se_{38} \cdot 2PhNHCOMe \cdot 15EtOH$ (8)

Of these compounds (2) to (6) contain iron clusters with 3D magnetic exchange interaction networks among iron ions. They have provided, by means of Mössbauer spectroscopy with a characteristic measurement response time $\tau_m = 10^{-8}$ sec, the first experimental observation confirming theoretical predictions that the appearance of collective magnetic phenomena occur at the vicinity $n \approx 10$, where n is the number of interacting spins in a cluster.

Magnetization measurements on compound (4), with the iron ions primarily in the Fe^{2+} state, show hysteresis effects at temperature 1.5 K and below attesting to the presence of collective magnetic correlations and particle-like behavior of these molecules.

Compounds (1), (7) and (8) contain iron clusters whose magnetic exchange interaction networks are essentially one-dimensional. For these, it was determined that if collective magnetic phenomena are present they must have a fluctuation time $\tau_s < 10^{-8}$ sec at 1.8 K and, therefore, Mössbauer spectroscopy down to pumped liquid helium temperatures has failed to detect them.

The synthesis and characterization of these nanophase structures are of great interest in increasing our understanding of the nature of the chemical bond and delocalized electronic states, as models for the study of bulk phenomena and as benchhmarks of theoretical approaches. In addition, they may lead to the synthesis of new materials, in the size range where convergence to the bulk value has not yet been attained, with novel electronic and magnetic properties, and the potential of technological utility. The iron-oxo clusters also present interest as synthetic analogue or model systems of biomineralization processes such as the accumulation of iron mineral nanophases by the iron storage protein ferritin.

I. Introduction

The disciplines of atomic and molecular physics on the one hand and solid state science on the other have been advanced for a long time by separate groups of investigators adhering to separate experimental approaches and theoretical methodologies. Cluster science is a fairly young discipline that concerns itself with the molecular/solid-state phase boundary, with impact on a diverse number of subdisciplines of chemistry, physics and materials science, which has brought together a diverse group of investigators. The electronic and magnetic properties of small (< 10 Å in size) metallic clusters, for example, are of considerable current interest because of commercial applications in heterogeneous catalysis[1] and high-density magnetic memory devices[2] and because of an intrinsic interest in the ways they are related to the bulk band structures and surface states of the corresponding crystalline metals. Semiconductor nanostructures are of intense current interest because of their potential use in the emerging field of nanotechnology [3].

Band structure calculations and other theoretical studies of crystalline materials are based on the assumption of long-range crystalline order, Bloch's theorem and reciprocal or k space representations which do not apply to small clusters where there is at most only short-range order. Molecular orbital (MO) theory, on the other hand, is well suited, in principle, for describing metal cluster electronic structure but is limited by the accuracy of available computational techniques. The quantum mechanical description of metallic clusters in terms of electronic energy level structure and spin density calculations has been rigorously pursued since the mid-1970's[4] while experimental observations to test theoretical predictions have appeared only since the mid-1980's, primarily due to the rapidly developing field of cluster beams [5].

Early molecular orbital calculations by Messmer *et al.*[6] using self-consistent-field-Xa scattered-wave methods on Cu, Ni, Pd and Pt clusters indicate a fast convergence of the discrete energy levels associated with the molecular state to the electronic density of states for the corresponding crystalline metals, obtained through band structure calculations. As shown in Fig. 1, MO calculations predict that a cluster of only 13 Cu atoms already possesses an electronic structure similar to that of the extended solid. Similar calculations on Ni_8, Ni_{13}, Pd_{13}, and Pt_{13} clusters indicate that Ni_8 and Ni_{13} clusters are magnetic while Pd_{13}, and Pt_{13} are not. It is remarkable that for the 13-atom clusters which have the same number of valence electrons, theory predicts Ni to be

magnetic and Pd and Pt to be nonmagnetic, consistent with the behavior found in the bulk metals.

Calculations on iron clusters by Yang *et al.*[7] also indicate that the dominance of magnetic effects on the electronic structure is quickly established. For Fe_{15} all of the major features of the bulk density of states are present in the cluster. Spin density maps generated for Fe_{15} bear a striking resemblance to those derived from neutron scattering experiments on bulk iron[8] (see Fig. 2). They also show new features that are absent in the extended solid or the molecular state. Indeed, experimental efforts to control the size and dimensionality of materials by growing them as clusters, multilayered and modulated structures[9], have produced systems with novel electronic and magnetic properties exhibiting quantum size effects.

An increasing number of experimental studies of the development of the electronic band structure of a solid with increasing cluster size have appeared in the literature since the mid-1980's, with results generally confirming theoretical predictions. Figures 3 and 4 present two examples. Ultraviolet photoelectron spectra of mass-selected copper clusters from a supersonic cluster beam[10] show the evolution of the 3d-band while the ^{77}Se NMR spectra of CdSe-R clusters[11] are seen to be shifted towards that of bulk cubic CdSe, rather rapidly, with increasing cluster size. In contrast, experimental investigations of the magnetic properties of metallic clusters have been rather limited, with only a handful of experiments on free iron and cobalt clusters[12]. Direct experimental observation of collective magnetic interactions — that is, short-range intracluster magnetic ordering — in nanometer-size clusters has been hindered by the difficulty of obtaining isolated, well-characterized clusters of such extremely small and uniform size.

Recently, new synthetic strategies in inorganic chemistry, utilizing controlled synthetic pathways, have yielded novel chemical structures[13-21] in the nanometer-size range which lie at the boundary between the molecular and the solid state that are structurally well characterized and crystallographically isolated, providing experimental systems appropriate for the investigation of the onset of collective magnetic phenomena associated with the solid state. (See Materials Section below)

With the caviat that the magnetic structure of metallic clusters is determined through direct d-d exchange interactions between atoms, while in molecular complexes magnetic ions interact through indirect superexchange via intervening ligands, the study of these complexes constitutes a novel and separate approach, than that of cluster beams, to the much debated subject of the transition from the molecular to the solid state. These nanostructures have the clear advantage of providing well-characterized systems

amenable to experimental investigation under extreme conditions of low temperatures and various applied magnetic fields, where quantum mechanical properties such as collective phenomena and quantum size effects may be observed. In addition, this approach has also produced molecular complexes where the magnetic interactions between iron ions are confined in a plane or a chain, which constitute finite analogues of lower dimensional magnetic solids [18,20,21].

In the solid state, magnetic exchange, magnetic anisotropy, and magnetic dimensionality are important factors in the process of magnetic ordering and in the type of excitation mechanism that the magnetic structures can sustain [22]. The molecular field approximation has been highly successful in describing the overall properties of 3-D magnetic substances, but breaks down completely in describing lower dimensionality magnetic phenomena. The failure of the molecular field model to describe accurately magnetic ordering in one and two dimensions lies in the fact that it ignores short-range order correlation phenomena leading to low-lying magnetic excitations known as spin-waves [23].

Most lower dimensionality magnetic solids do not undergo long-range order until very low temperatures are realized, when the weak inter-chain or inter-layer exchange forces become important enough to drive 3-D ordering. Crystallographically isolated molecular clusters of an increasing number of exchange-coupled ions confined in a plane or in a chain may serve as finite analogues of pure 2-D or 1-D magnetic systems. Depending on the degree of isolation from neighboring clusters, there may be no intercluster exchange and thus no 3-D ordering will be expected at any temperature. Thus, these clusters may exhibit interesting short-range correlation effects and may be natural candidates for basic research in this field. Indeed, a great deal of the theoretical work in 1-D magnetic systems has been done on hypothetical finite antiferromagnetic chains or rings [24,25].

Theoretical calculations of the spin-wave spectra of the antiferromagnetic linear chain, eigenstates of the isotropic Heisenberg exchange Hamiltonian with periodic boundary conditions, have been carried out for N=6, 8, 16, and 48 and have been compared to that of an N=∞ chain [24], N is the number of exchange-coupled spins in the chain. Fast convergence to the spectrum of the infinite chain is observed with increasing N. For N=16 the calculated spectrum approximates quite closely that obtained for the N=∞ case. For N=48 the spin-wave spectrum almost completely overlaps the N=∞ case (see Fig. 5).

Experimental confirmation of the above predictions presents a special challenge to the experimentalist because observation of collective magnetic correlations, that is short-range magnetic ordering, in small particles or clusters and lower dimensional magnetic systems is difficult to detect due to superparamagnetic-relaxation[27,28] and spin-fluctuation[29] phenomena, respectively, which result in very short spin-relaxation times, τ_s. As a consequence, the observation of the onset of magnetic ordering phenomena in nanometer-sized macromolecular structures would depend critically on the characteristic measuring time, τ_m, associated with the particular experimental technique used and the lowest temperatures experimentally achievable. A fast spectroscopy is required with a measuring time much shorter than the spin relaxation time ($\tau_m << \tau_s$) and ultra-low sample temperatures.

Spin-coupled iron complexes have been chosen as experimental test systems because their magnetic properties can be studied not only by magnetic susceptibility measurements, but also by Mössbauer spectroscopy. The characteristic measuring time for Mössbauer spectroscopy is $\tau_{Möss} \sim 10^{-8}$ sec while that for magnetic susceptibility measurements is often $\tau_{Mag} \sim 1$ sec. Thus, Mössbauer spectroscopy can probe dynamical spin-fluctuation phenomena while susceptibility studies give only averaged magnetic moment information. This approach has led to the first experimental study which has allowed confirmation of theoretical predictions that collective magnetic phenomena, responsible for magnetic ordering in solids, first appear at the vicinity of $n \approx 10$, where n is the number of interacting spins in a 3-D cluster. In contrast, clusters of lower magnetic dimensionality containing up to twenty exchange coupled iron ions have failed to produce such correlation effects within the Mössbauer time window at temperatures down to 1.6K.

II. Materials

Controlled hydrolytic polymerization of iron in nonaqueous solvents has led to the synthesis of rare, discrete polyiron oxo-hydroxo complexes of increasing iron-nuclearity in which the superexchange interaction networks are either three-dimensional[13,15] or one-dimensional.[18] Similarly, self-assembly reactions in nonaqueous solvents has produced polynuclear iron-sulfide and selenide complexes of nanometer size in which the intracluster superexchange pathways are essentially one-dimensional[17,19,20].

1. Molecular Clusters of 3-D Magnetic Dimensionality. Iron polymerization in aqueous solutions results in the uncontrollable formation of mixtures of high molecular weight polymers[30]. The generation of monodispersed oxo-hydroxo-iron nanoclusters requires a competitive reaction chemistry between core cluster growth to form a bulk material and cluster encapsulation by terminal ligation that arrests further core growth. By using aprotic solvents as the reaction medium and adding water, needed for hydrolysis, and an organic base in limited quantities, a certain degree of control of the extent of polymerization and resulting size of the clusters can be achieved. Structurally characterized complexes of nuclearity Fe_3, Fe_4, Fe_6, Fe_8 and Fe_{11} made of $[Fe_2O]^{4+}$ and $[Fe_3O]^{7+}$ building blocks have been reported in the literature[31]. These complexes have been investigated as possible intermediates[14] in a biomimetic approach to the study of the iron nucleation process by ferritin, the iron storage protein in mammalian and bacterial life forms[32]. In this case encapsulation of the iron-oxo-hydroxo mineral phase in nanometer-sized particulate form is done by the protein shell, which forms an interior cavity of ~70Å diameter where up to 4,500 iron atoms can be reversibly stored.

The structure of the undecanuclear complex $[Fe_{11}O_6(OH)_6(O_2CPh)_{15}] \cdot 6THF$(2) is shown in figure 6. All metal atoms are six-coordinated, of distorted octahedral symmetry, and all donor atoms are oxygen from oxo, hydroxo and benzoate groups where the latter surround and encapsulate the central iron-rich core. Further polymerization of this structure has provided large mixed-metal, mixed-valence complexes of the form $[Fe_{16}MO_{10}(OH)_{10}(O_2CPh)_{20}]$, where M is a divalent transition metal ion. Structures with M = Mn^{2+}, Co^{2+}, and Fe^{2+} have been isolated. Figure 7 shows the structure of the $[Fe_{16}Mn]$ (5) cluster. The structure is centrosymmetric with a Mn^{2+} ion located at the center of symmetry. This Mn^{2+} ion forms the shared corner of an $\{[Fe_3O_3(OH)]_2Mn\}$ double cube which is surrounded by an $[Fe_{10}O_4(OH)_8]$ cage and this in turn is encapsulated within a shell of 20 benzoate ligands. Further details on the synthesis and x-ray structure of these molecules have been reported previously[13-15,21]. The Fe_{17} cluster (6) is believed to have a structure analogous to (5) with a Fe^{2+} ion replacing the central Mn^{2+} ion. No crystal structure determination of the Fe_{17} molecule has been obtained so far but elemental analysis and other spectroscopic data supports this hypothesis .

These are neutral molecules forming crystals by Van der Waals forces. The bulky benzoate ligands that encapsulate the central exchange-coupled ion cores, which are ca. 10 Å in diameter, keep the cores magnetically isolated from one another. The packing of the central iron core within the crystal for compound 2 is shown in Fig. 8. The resulting average distance between centroids is ~20Å, over which intercluster magnetic

interactions are negligible. Similar core distances are found in the crystal stacking of compounds 5 (not shown). Thus, any magnetic ordering effects observed should be due to intramolecular spin interactions rather than long-range magnetic order throughout the crystal (vide infra).

Although the mechanism by which the $[Fe_{16}M]$ clusters are assembled has not been established, they may formally be constructed by fusion of two molecules of $[Fe_{11}O_6(OH)_6(O_2CPh)_{15}]$. Each Fe_{11} cluster first loses a $[Fe_3O(OH)(O_2CPh)_5]^+$ fragment. The remaining $[Fe_8O_5(OH)_5(O_2CPh)_{10}]^-$ fragments then combine in the presence of a divalent ion, M^{2+}, to form the larger cluster[15] (see Fig. 9). This is the most likely route by which the $[Fe_{16}M]$ clusters may be obtained. Further growth of polymetal oxo-hydroxo structures can be envisioned by repeating the basic step of Fig. 9 leading, conceivably, to the synthesis of extended structures containing 5n+11 iron ions with n = 0,1,2, etc. Efforts to isolate and characterize larger clusters are in progress.

Following a modified approach for the synthesis of extended iron oxo-hydroxo structures with the iron ion primarily in the reduced Fe^{2+} state (see figures 10 , 11 and 12) has led recently to the synthesis of dodecanuclear clusters; a polymeric one of the general formula $Li_2[Fe_{12}(O)_2(OCH_3)_{14}(O_3CCH_3)_{10}(CH_3OH)_2]$(3) shown in figures 10 and 11 and a discrete one $[Fe_{12}(O)_2(OCH_3)_{18}O_2(CCH_3)_6(CH_3OH)_4$ (4) shown in figure 12. These are mixed valent complexes with 3 containing $2Fe^{3+}$ions at the center of the structure as indicated in figure 10 with the rest being in the Fe^{2+} state. Charge neutrality is provided by the association of 2Li ions per molecule which also provide weak bonds between clusters producing a polymerized structure. Compound 4 contains $4Fe^{3+}$ ions as indicated in figure 12. The higher degree of iron oxidation ensures charge neutrality without the need of an additional metal ion. These structures present a nanometer-sized crystalline lattice whose extension to an extended lattice is easier to envision than those in compounds 2, 5, and 6.

2. Molecular Clusters of Low Magnetic Dimensionality.

Iron polymerization in non-aqueous solvents has also produced the compound $[Fe(OMe)_2(O_2CCH_2Cl)]_{10}$ (1) reported recently[18]. This compound assembles in methanolic solutions of diiron (III) oxo complexes and consists of 10 ferric ions arranged in a circular array (see Fig. 13). The 10 iron ions are essentially coplanar with an average deviation of ±0.005 Å from the best least square plane through them. Each iron atom has a distorted octahedral geometry and is joined to its neighbors by edge-sharing methoxide and cis-carboxylate bridges, forming a molecular ferric wheel of 12 Å in diameter. It

provides an excellent experimental system for testing theoretical predictions of ref. 24 discussed in the introduction. (See Fig. 5.)

Iron sulfur chemistry has also led to the synthesis of novel macromolecular structures where Fe is tetrahedrally coordinated to sulfur atoms and arranged in lower dimensional magnetic structures[17]. The fundamental building block in these systems is the Fe_2S_2 rhomb 1 shown in Fig. 14 In a purely conceptual but highly instructive way we see in Fig. 14 the possible geometrical arrangements obtained by the fusion of Fe_2S_2 rhombs by edge- and vortex-sharing to produce dimeric, trimeric, tetrameric, and extended iron sulfur structures. Although, in its more general occurrence rhomb 1 is dimensionally variable, being found in both planar and non-planar conformations, it is seen that a number of lower dimensional — topologically and magnetically — structures are possible, some of which are similar to those encountered in extended structures of some Fe chalcogenide phases[17].

The highest nuclearity FeS cluster produced to date by self-assembly reactions in non-aqueous solvents is the cluster $[Na_2Fe_{18}S_{30}]^{8-}$(7) shown in Fig. 15. It has a disk-like topology with dimensions 13.3 x 16 Å, maximum thickness of 3.3 Å and no terminal ligation. The structure closes upon itself obviating the need for terminal ligation to arrest further growth, a situation, albeit of lower dimensionality, analogous to that of the resonant closed shell structures of the fullerene carbon molecules[33]. All iron ions in 7 are confined in a plane. Two sodium ions are bound to the interior sulfur atoms of the cluster, partially balancing out the high negative electronic charge on the $Fe_{18}S_{30}$ ring. The cluster is stabilized as the anion in the crystal $(Pr_4N)_6Na_4Fe_{18}S_{30}\cdot 14MeCN$. The crystal structure consists of discrete Pr_4N^+ ions and two additional Na^+ ions weakly associated with cluster 7. Further details on the synthesis and structure of this complex have been reported elsewhere[17]. The ring molecules pack in the ionic crystal (Fig. 16) with only translational symmetry, which results in parallel layers of anions similar to those found in many chalcogenide binary phases. Average distance between ring molecules is about 20Å. This system can serve as a finite analogue of extended lower magnetic dimensionality layered structures.

Analogous FeSe chemistry has led to the production of another closed chemical structure, an unprecedented Fe_{20} cluster[19,21] of stoichiometry $[Na_9Fe_{20}Se_{38}]^{9-}$(8) shown in Fig. 17. It has a bicyclic structure of ellipsoidal shape. The structure is built up from Fe_2Se_2 rhombs which form three short linear FeSe segments connected together at the ends by vertex-sharing and edge-fusion. Nine sodium ions are encapsulated within the cluster cavity. The cluster approaches D_{3h} symmetry with a pseudo-C_3 axis along the

Fe(10)-Fe(10') vector. Cluster dimensions are 17.4 Å [Se(1)-Se(1')] x 11.2 Å [2(centroid-Se(6))]. The resulting structure, while topologically three-dimensional, represents a rare example of a finite 1-D magnetic system. Iron ions are strongly exchange-coupled through the bridging Se atoms along linear segments, but lack any bridging atoms between chains. The cluster is stabilized within an ionic crystal with stoichiometry $(Bu_4N)_{4.5}$ $Na_{13.5}Fe_{20}Se_{38}$·2PhNHCOMe·15EtOH. Further details on the synthesis and structure are given elsewhere[19,20].

III. Experimental Methods

The electronic and magnetic properties of these nanophase iron complexes have been examined through Mössbauer spectroscopy and magnetic measurements. Susceptibility and saturation magnetization measurements are sensitive to the averaged total magnetic moment of the clusters and constitutes a macroscopic magnetic characterization of the system. Mössbauer spectroscopy, on the other hand, probes the local moments at the iron nuclei, the iron oxidation state, degree of charge and spin localization (or delocalization), the existence of mixed valence, and the distribution of magnetic moments among various iron sites. This comprises a microscopic electronic and magnetic characterization of the system. Through Mössbauer spectroscopic methods we determined:

1) the isomer shift δ, which is a measure of the s-electron density at the iron nucleus and is sensitive to the oxidation state of the iron ions in the cluster, and

2) the qudrupole splitting ΔE_Q, which measures the electrostatic interaction of the quadrupole moment of the first excited state of the ^{57}Fe nucleus and the surrounding electronic charge distribution, and is sensitive to the coordination symmetry at the iron site, and

3) the internal magnetic hyperfine field H_{eff}, which is proportional to the spin expectation value of the iron ion and, therefore, the local magnetic moment at the iron sites.

In addition, as mentioned in the introduction, owing to the relatively short characteristic measuring time of Mössbauer spectroscopy, $\tau_{Möss} \sim 10^{-8}$ sec, dynamical magnetic characterization can be performed, i.e., slow-spin[34] superparamagnetic relaxation[27,28] and lower dimensionality spin-fluctuation processes[29] can be studied. The internal magnetic field at the iron nucleus depends on the number of unpaired electrons surrounding the nucleus. Whether the magnetic field is observable by Mössbauer spectroscopy depends on the relaxation time of the unpaired 3d electron spin as compared with the characteristic measuring time of the Mössbauer technique. For $\tau_S > \tau_{Möss}$, a

magnetically split six-line spectrum is observed. For $\tau_S < \tau_{Moss}$, the average magnetic field at the nucleus is zero and no magnetic structure is observed. For $\tau_S \approx \tau_{Moss}$, transitional spectra showing magnetic relaxation broadening are seen.

The application of external magnetic fields is not a prerequisite for the observation of Mössbauer spectra, unlike related techniques such as NMR, EPR and magnetization measurements. This is an advantage since one need not rely on data extrapolated to zero field[35]. Mössbauer spectroscopy in external fields of various magnitudes has also extensively been used in this investigation because magnetically perturbed spectra unravel new and important information about the structural, electronic and magnetic properties of the system under study. In particular, perturbation of the Mössbauer spectra by an external field provides the means for distinguishing between magnetic ordering and slow spin relaxation phenomena. In the presence of an external field magnetic anisotropies, spin canting and spin reorientation phenomena can easily be studied[36,37].

Magnetization measurements were performed with a SHE SQUID magnetometer in the temperature range $1.8 \leq T \leq 300K$ and applied field range $0 \leq H_o \leq 50KOe$ and by use of a Foner Vibrating Sample Magnetometer (VSM) associated with the Bitter electromagnet high field facility at the Francis Bitter National Magnet Laboratory affording applied magnetic fields up to 200KOe and temperatures down to 0.6 K (pumped liquid ^3He). Mössbauer measurements were performed with a conventional constant acceleration spectrometer with variable temperature, $1.8 \leq T \leq 300K$, and a longitudinal applied magnetic field, $0 \leq H_o \leq 80KOe$, capability. Experimental spectra were fit using standard fitting procedures to theoretical spectra including distribution of internal magnetic fields. Isomer shifts are given relative to metallic iron at room temperature.

IV. Results and Discussion

1) *3D Molecular Clusters*. Mössbauer and magnetic measurements on complexes 2, 5 and 6 have been completed and these results are discussed first. Preliminary data on compounds 3 and 4 are presented later.

Variable-temperature magnetic susceptibility studies for clusters 2, 5, and 6 in the temperature range from 2K to 300K performed with a SQUID magnetometer showed paramagnetic behavior (Figs. 18,19, 20). A sharp increase in μ_{eff} with temperature was observed indicative of a net antiparallel spin coupling within the aggregate $[Fe_{11}]$ and

[$Fe_{16}Mn$] and [Fe_{17}] molecular cores and the existence of low-lying magnetic excited states. These arise from the complex superexchange magnetic interaction network established through oxo, hydroxo and benzoate-group bridging pathways; μ-oxo bridges between high spin ferric ions have typical exchange integrals of the order of $J \approx -100cm^{-1}$. Hydrogenation of the bridge has been observed to drastically reduce their exchange integrals to only about $J \approx -10cm^{-1}$ [38]. These interactions would produce an antiparallel-spin-coupled system with a dense ladder of excited spin states[39] . Extrapolation of μ_{eff} values to zero temperature (not shown) give ~1.9 μ_B and ~5.9 μ_B per cluster for 2 and 5, respectively, approximating a ground electronic net or total spin state for complex 2 of $S_T=1/2$ and for 5of $S_T=5/2$ by use of the relationship $\mu_{eff} = [g^2S(S+1)]^{1/2}$ and assuming g=2 . At room temperature the effective moment for cluster 2 has saturated at a value of 14.6μ_B per molecule (see figure 18) while for cluster 5 μ_{eff} ~ 13.5μ_B per molecule and still increasing (see Fig. 19).. The Fe_{17}(6) cluster gives a $\mu_{eff} \approx 4.8\ \mu_B$/cluster at zero temperature indicating a ground total spin state of $S_T=2$.and $\mu_{eff} \approx 13.5\mu_B$ at room temperature (see figure 20) and still increasing.

High-field magnetization studies using a VSM magnetometer in a water-cooled Bitter electromagnet up to 230KOe, reveal a monotonic increase of cluster moments up to the highest field without reaching saturation (Figs. 21,22,23). There is no hysteresis in the magnetization, and no remnant moment for any of the three clusters when the field is swept up to 230KOe and back down to zero. An interesting step in the magnetization vs. applied field functional dependence reminiscent of a spin-flop magnetic phase transition[40] is observed for 2 which is absent in 5 or 6 (vide infra).

Mössbauer spectra of polycrystalline samples at T = 80K are paramagnetic and show a symmetric quadrupole doublet with an isomer shift δ = 0.50 mm/sec and a quadrupole splitting ΔE_Q = 0.91 mm/sec for the [Fe_{11}] cluster, δ = 0.51 mm/sec, ΔE_Q = 0.77 mm/sec for the [$Fe_{16}Mn$] cluster and δ=.48mm/sec and ΔE_Q=0.82mm/sec at T=20k for [Fe_{17}] typical of high spin S=5/2, Fe^{3+} ions. The isomer shifts are comparable to those of oxo-bridged high spin ferric complexes, but the quadrupole splittings are smaller than those observed for oxo-bridged complexes (1.5-2.0 mm/sec)[41] and approach those reported for iron-oxide and iron- hydroxide particles[42-44].

At 4.2K the Mössbauer spectrum of compound 2 is dominated by intermediate relaxation phenomena (Fig. 24). It is significantly broadened, with wings that extend from about -7 to +7 mm/sec, but no magnetic hyperfine lines are defined even at 1.8K. The net moment of the Fe_{11} aggregate does not have a fixed spatial orientation in zero field but fluctuates with a certain frequency with respect to the crystal axis. The

broadening of the Mössbauer spectrum implies that the relaxation time is of the order of the Mössbauer time scale which is given by the ^{57}Fe nuclear Larmor precession frequency, $\nu_L = (g_n\mu_n/h)H_{eff}$ where g_n is the nuclear g-factor of the first excited state of ^{57}Fe, μ_n is the nuclear magneton, h is the Planck constant, and $\mathbf{H}_{eff}$ is the effective field at the nucleus. For high-spin ferric ion $\mathbf{H}_{eff} \approx 500$ KOe, which gives $\nu_L \sim 3.9 \times 10^7$ sec^{-1} or, equivalently, a relaxation time $\tau_L \sim 2.5 \times 10^{-8}$ sec. Shorter relaxation times at higher temperatures obscure the magnetic hyperfine broadening.

In contrast, compound 5 exhibits relaxation phenomena in its Mössbauer spectra, appearing at T ≅7K, with magnetic hyperfine lines developing below 6K superimposed on a broad absorption envelope at the center of the spectrum (Fig. 25). With decreasing temperature the intensity of the magnetic subspectrum increases at the expense of the central doublet. At 1.8K a well defined magnetic, six-line absorption spectrum is obtained indicating that the complex has crossed from fast to slow relaxation behavior on the Mössbauer time scale. The $[Fe_{17}]$ cluster shows superparamagnetic behavior at low temperatures with spectra at 2K (the lowest temperature measured) still showing a superposition of quadrupolar and magnetically split subspectra (Fig. 26) Interestingly, at high temperatures no distint ferrous ion Mössbauer absorption is observed which indicates that the sixth 3d electron of the central, formally Fe^{2+}, ion in the structure is delocalized.

Figures 27, 28 and 29 show spectral behavior in the presence of an external magnetic field $\mathbf{H}_o$ = 60 and 80 KOe applied parallel to the direction of the 14.4 KeV γ- ray for compound 2 and 5, and Ho=60KOe for (6), respectively. In the presence of the field the total spin of the cluster is forced to precess about $\mathbf{H}_o$, further reducing its relaxation time. Thus, while at 4.2K in zero field all three compounds 2 and 5 and 6 exhibit a strong absorption doublet at the center of the spectrum (Figs. 24, 25 and 26), at the same temperature upon application of the field only magnetically split spectra are observed (Figs. 27, 28 and 29). The six lines in each spectrum correspond to the two $\Delta m = 0$ (lines 2 and 5) and the four $\Delta m = \pm 1$ lines of a magnetic hyperfine spectrum[44]. It is most notable that (a) upon application of the external field the middle $\Delta m = 0$ absorption lines persist and (b) the overall magnetic splitting, which is a measure of the total effective magnetic field at the iron nucleus, does not change significantly with increasing applied field.

The Mössbauer spectra in the presence of the external field carry a wealth of information about the magnetic structure of these molecules. In particular, they provide the means of distinguishing between slow paramagnetic relaxation and magnetic

ordering. The simplest example of the interaction between two magnetic ions is that which occurs in a dimer complex. The principle interaction of magnetic exchange, $H_{ex} = -JS_1 \cdot S_2$, is short-range and results in parallel or antiparallel spin alignment within the molecular complex[40]. In a three-dimensional crystalline lattice, however, the same pairwise exchange interaction leads to the transition from the paramagnetic state to a magnetically-ordered state with long-range correlation between magnetic moments[45]. Molecular paramagnetic systems respond to an applied field differently than magnetically ordered solids. In the study of paramagnetism the only preferred direction for spin polarization is that of the applied field, while in magnetic solids easy axes of magnetization within the crystalline structure determine the direction of local spin orientation until high enough fields are applied that overcome internal magnetic anisotropy energies[45].

Molecular complexes containing an even number of exchange coupled high-spin ferric ions produce simple Mössbauer spectra in the presence of an applied field, typical of diamagnetic complexes[46] where the only field at the iron nuclei is that of the applied field, H_0. Complexes containing an odd number of exchange-coupled high- spin ferric ions produce complex Mössbauer spectra[47] in the presence of external fields governed by the Hamiltonian of equation 2 where $\langle S_T \rangle$ is the expectation value

$$H = H_{ex} + g\beta \mathbf{H_0} \cdot \langle S_T \rangle - g_n \beta_n \Sigma_i \mathbf{I_i} \cdot \mathbf{H_{ni}} \qquad (2)$$

of the total electronic spin of the cluster, produced by the strong intracluster exchange interaction H_{ex}, and $\mathbf{H_{ni}}$ is the total magnetic field at the ith nucleus of nuclear spin $\mathbf{I_i}$. All other symbols have their usual meaning. The second term gives the electronic and the third the nuclear Zeeman interaction, where the total magnetic field at the ith nucleus is given by the vector sum of the applied, $\mathbf{H_0}$, and hyperfine magnetic field, $\mathbf{H_{hi}}$, due to the unpaired 3d electrons[44] (Equ.(3)). Because high-spin ferric ions are

$$\mathbf{H_{ni}} = \mathbf{H_0} + \mathbf{H_{hfi}} \qquad (3)$$

highly isotropic, local spins project along the direction of the total spin of the cluster, $\mathbf{S_T}$, which in turn aligns in the direction of the applied field, producing a total internal field at the iron nuclei parallel to the direction of $\mathbf{H_0}$ and, therefore, to that of the γ-ray. Selection rules for the magnetic dipole Mössbauer transition then dictate that the $\Delta m=0$ lines (lines 2 and 5) approach zero intensity[44].

The nonvanishing $\Delta m = 0$ lines in Figs. 27, 28 and 29 indicate that even though the total moment of the cluster may be aligned along the direction of the magnetic field, the hyperfine fields, and therefore the local magnetic moments, at the different iron sites are not colinear with the total moment or $\mathbf{H}_0$, but tend to lie perpendicular to it and, therefore, to the total spin of the cluster. That is, internal magnetic anisotropies dominate, with local spins projecting along preferred crystalline axes rather than the direction of the applied field, $\mathbf{H}_0$. Single ion anisotropy cannot be invoked since the $3d^5$ electronic state for high spin Fe^{3+} is highly symmetric as discussed above. Rather, their presence points to collective magnetic interactions producing short-range magnetic ordering and the existence of easy directions of magnetization within the crystalline solid. They point to a noncolinear antiferromagnetic structure or canted antiferrimagnetic order of the type observed in oxidic spinels[48] or the surface atoms of antiferromagnetic small particles[36]. In a cluster containing a number of the order of ten interacting spins, almost all spins lie at the surface and surface effects should dominate. It could also be a result of frustration in the network of magnetic interactions present resulting in a spin-glass-like structure[49]. There is no long-range spatial correlation of the antiferromagnetic axis of a cluster with its neighbors since clusters are separated by a distance of ~20Å, over which long-range dipole-dipole interactions are negligible[50]. Thus, the magnetic domain size must be confined within the Fe_{11} or $Fe_{16}M$ cores. A broad transition to a six-line absorption spectrum is observed in the zero-field Mössbauer spectra of $Fe_{16}Mn$ (Fig 25) and of Fe_{17} (Fig.. 26) superimposed on a relaxation envelope. The positions of the outer absorption lines, which give a measure of the observed hyperfine magnetic field H_{hf}~400KOe, are independent of temperature, a behavior reminiscent of the superparamagnetism of single-magnetic-domain particles (<100Å) of antiferromagnetically-coupled ferric oxides and hydroxides[42,43].

Let us compare the results shown in Figs. 25 and 26 with those of magnetically ordered fine particles[36,42,43]. In a fine, antiferromagnetically ordered particle with uniaxial anisotropy, thermal energies can excite relaxation of the antiferromagnetically ordered spins to the opposite configuration ($\uparrow\downarrow\uparrow\downarrow...\uparrow\downarrow\uparrow\downarrow...$) which is energetically equivalent. Thus, the magnetic moment of such ultrafine particles undergoes, above a certain temperature, spontaneous reversals, analogous to the behavior of paramagnetic atoms, exhibiting the so-called superparamagnetic behavior[27,28]. The relaxation time which measures how rapidly transitions between the two configurations, or spontaneous moment reversals, occur is given by equ. 4, where K is

$$\tau_S = \tau_0 \exp(2KV/kT) \qquad (4)$$

the magnetic anisotropy constant and 2KV is the anisotropy energy barrier for a particle of volume V that measures the energy required to go from one easy direction of magnetization to the other, k is Boltzmann's constant and T is the temperature. τ_0 is a constant characteristic of the material of the order of the 10^{-9}sec[42]. The Mössbauer spectrum of a system where τ_S is fast with respect to the Mössbauer time scale is a doublet, while that of a slow relaxing system is a sextet. The characteristic time $\tau_{Möss}$ is given by the ^{57}Fe nuclear spin Larmor precession time, τ_L, of the 14.4 KeV energy state in the hyperfine field at the nucleus. For $H_{hf} \sim 400$KOe, as observed for compound 5, $\tau_L \approx 3.2 \times 10^{-8}$ sec. The temperature at which the system changes from the fast to the slow relaxation regime, i.e. at $\tau_S = \tau_L$, is known as the blocking temperature, T_B. For 5, using equation 4, analysis of the temperature dependence of the Mössbauer spectra gives $T_B \approx$ 4K, while for 2 $T_B <$ 1.8K. For 6 $T_B \approx$ 2K. Since clusters 5 and 6 have similar volumes, the difference in T_B points to a higher anisotropy constant K for 5 as compared to 6.

The basic difference between the present Mössbauer study of well defined molecular clusters, and thus of a single volume, and those of fine particles available in the literature[42,43] is that the latter deal with a broad distribution of particle sizes giving rise to very broad transitions from the doublet to the six-line spectrum. The breadth of the transition has often been used to determine the distribution of particle sizes present in the sample, assuming an infinitely sharp transition for each particle volume[42]. Theory predicts, however, that, as observed here, even single particle volume samples may exhibit narrow transitions but of finite sharpness, the latter being inversely proportional to the saturation magnetization of the bulk material[28].

The spectra of Figs. 27, 28 and 29 have been least-squares fitted, assuming a distribution of total internal magnetic fields, superimposed on a broad background, in order to simulate relaxation effects[28]. For Fe_{11}, an average internal field of $H_n \equiv$ 430KOe is observed while for $Fe_{16}Mn$ this value is reduced to 400KOe and for the Fe_{17} to 380 KOe. This reflects higher d-electron localization in the smaller Fe_{11} cluster compared to $Fe_{16}Mn$ and Fe_{17}, in agreement with the trend observed in Stern-Gerlach experiments on free iron clusters and theoretical calculations[12].

A close comparison of Figs. 27and 28 indicates that, in going from H_0 = 60KOe to H_0 = 80KOe, the center of the distribution of the internal fields remains unaffected, but the detailed shape of the distribution and, therefore, that of the local magnetic moments, changes for the Fe_{11} clusters, while that of $Fe_{16}Mn$ exhibits a slight broadening but

otherwise remains undisturbed. In the 80KOe Mössbauer spectra of Fe_{11}, wings at the outer absorption lines appear, indicated by the arrows in Fig. 27(a). The observed changes in the internal field distributions in Fig. 27(b) to higher and lower internal magnetic field values, are consistent with the onset of local spin polarization along the applied magnetic field, a behavior reminiscent of antiparallel-spin-coupled iron molecular paramagnetic complexes where, due to spin colinearity an increasingly resolvable separation of spin-up (relative to $\mathbf{H_o}$) and spin-down magnetic subspectra is produced with increasing values of the applied field[47]. Thus, the Fe_{11} cluster seems to be at the boundary of molecular/solid-state magnetic behavior, while the $Fe_{16}Mn$ and the Fe_{17} cluster clearly exhibit "particle-like" magnetic behavior. The onset of local spin polarization along H_o for Fe_{11} at 80KOe applied field coincides with the step in the magnetization vs. applied magnetic field behavior of Fig. 21.

The iron clusters discussed so far contain iron ions exclusively or primarily in the high spin ferric state (S=5/2, Fe^{3+}). The dodecanuclear iron clusters 3 and 4 contain iron primarily in the reduced state. Compound 3 contains ten ferrous and two ferric ions as supported from crystallographic and Mössbauer data. Figure 30 shows Mössbauer spectra of $[Fe^{2+}_{10}Fe_2^{3+}(O)_2(OCH_3)_{14}(O_2CCH_3)_{10}(CH_3OH)_2]Li_2$ (3) at various temperatures. At T=20 K fast relaxing spectra are observed composed of two overlapping quadrupole doublets with $\delta_1 = 0.52$, $\Delta E_{Q1} = 0.7$ mm/sec and $\delta_2 = 1.26$ and $\Delta E_{Q2} = 2.53$ mm/sec corresponding to high spin ferric and high spin ferrous ions consistent with crystallographic data.

Below 15 K magnetic hyperfine structure appears with a magnetic hyperfine field of the order of $H_{hf} \approx 515$ KOe, corresponding to high-spin ferric ions. The ferrous quadrupole doublet broadens but no distinct ferrous magnetic hyperfine lines appear until temperatures below 6 K. The appearance of a collapsed broad absorption line at about 1.5 mm/sec accompanies the onset of magnetic relaxation effects, indicating that part of the absorption spectrum arises from iron ions undergoing intermediate relaxation phenomena compared to the Mössbauer time scale. Spectra down to 2 K show the appearance of a second but much broader magnetic hyperfine spectrum with $H_{hf} \approx 435$ KOe and the persistence of both a broad ferrous quadrupolar doublet and a collapsed ferrous absorption line at the center of the spectrum.

The data of Figure 30 is very preliminary and is still being analyzed. We would like to obtain Mössbauer data in the presence of an external magnetic field which may give additional information about the nature of the magnetic ordering observed. Magnetization

measurements are also being planned for complete magnetic characterization of the system.

The second dodecanuclear cluster 4 contains four ferric and eight ferrous iron ions $[Fe_4^{3+}Fe_8^{2+}(O)_2(OCH_3)_{18}(O_2CCH_3)_6(CH_3OH_4)]$ supported by crystallographic and Mössbauer data. Two distinct ferrous subsites are observed with different degrees of distortion from perfect octahedral coordination. Mössbauer data at T=20 K (see Fig. 31) fitted to the superposition of three quadrupole doublets give δ_1 = 0.47, ΔE_{Q1} = 0.74 mm/sec for the Fe^{3+} sites and δ_2 = 1.28, ΔE_{Q2} = 2.02 mm/sec and δ_3 = 1.29, ΔE_{Q3} = 3.29 mm/sec for the two Fe^{2+} sites. This structure also orders magnetically at low temperature, as seen in Fig. 31. At 6 K magnetic hyperfine lines appear corresponding to Fe^{3+} ions. Fe^{2+} subsites exhibit intermediate relaxation. Analysis of this data which has recently been obtained is in progress.

Magnetic studies on this system are presented in Figs. 32 and 33. Susceptibility and effective moment studies show paramagnetic behavior at high temperatures. At low temperatures, however, magnetization studies reveal the presence of hysteretic effects, associated with the solid state. This system is of single magnetic domain and thus hysteresis effects must be associated with shape anisotropies and rotation of the magnetization vector away fron an easy direction, rather than domain wall motion associated with hysteretic effects in extended solids. Their presence, however, attests to the existence of collective magnetic interactions within the 12-iron aggregate and particle-like behavior of this macromolecule. We are in the process of analyzing and interpreting this very interesting effect. To the best of my knowledge this is the first time that hysteresis effects have been observed in manometer-sized molecular systems.

The fact that the bigger $Fe_{16}Mn$ and Fe_{17} clusters showed no hysteresis must be a result of the presence of Fe^{3+} which is isotropic and that the clusters have more or less spherical shape. The Fe_{12} clusters contain primarily anisotropic Fe^{2+} ions and have spheroid rather than spherical shape.

2) Low-Dimensional Clusters. The decanuclear complex $[Fe(OCH_3)_2(O_2CCH_2Cl)]_{10}$ (1) presents a rare example of one-dimensional system in which all irons are in the Fe^{3+} state. Magnetization measurements indicate that the iron ions are antiferromagnetically coupled with a singlet (S_T = 0) ground state. Mössbauer spectra at 4.2 K shown in Fig. 34 show a single quadrupole doublet with δ = 0.52 mm/sec and ΔE_Q = 0.62 mm/sec. Lower temperature measurements are planned to be performed.

The Mössbauer spectra of the lower dimensional clusters, $[Fe_{18}S_{30}]$ (7) and $[Fe_{20}Se_{38}]$ (8) were examined in zero field at 1.6-180K and in a longitudinally applied magnetic field of 80KOe at 4.2 K. Mössbauer spectra obtained for the two clusters were very similar. Zero-field spectra at 4.2K for cluster 7 are shown in Fig. 35(a) and consist of two apparent overlapping doublet features. The minority component appears as a shoulder on the positive velocity side. No magnetic hyperfine structure was observed even at 1.6K, the lowest temperature studied. Spectral fits based on a two-site model give an isomer shift of $\delta_1 = 0.30$ mm/sec and a quadrupole splitting of $\Delta E_{Q1} = 0.81$ mm/sec for the majority iron component, and $\delta_2 = 0.46$ mm/sec and $\Delta E_{Q2} = 1.49$ mm/sec for the minority component. The cluster contains nine crystallographically distinct Fe sites, all of which are tetrahedrally coordinated iron to sulfur atoms whose subspectra are unresolved. It is a mixed-valence, even-electron system, having formally $14Fe^{3+}$ and $4Fe^{2+}$ ions. In the Mössbauer spectra no individual ferrous sites, for which $\delta = 0.5$-0.77 mm/sec and $\Delta E_Q \approx 3$ mm/sec, are observed. The cluster is electronically delocalized[17].

Zero-field Mössbauer spectra of 8 (not shown) are very similar to that of 7, with Mössbauer parameters of majority and minority components $\delta_1 = 0.38$ mm/sec, $\Delta E_{Q1} = 0.60$ mm/sec and $\delta_2 = 0.43$ mm/sec, $\Delta E_{Q2} = 1.15$ mm/sec, respectively[20].. This cluster is also of mixed valence of formally $18Fe^{3+}$ and $2Fe^{2+}$ ions. Electronic delocalization is also observed here. The spectrum of 8 in a longitudinally applied magnetic field, of 80KOe at 4.2K is shown in Fig. 35). This spectrum is characteristic of a diamagnetic ground spin complex as the field observed at the iron sites equals that of the applied field, H_o. Spectra of 7 looked identical to 8. Susceptibility measurements also indicate diamagnetic ground total spin states $S_T=0$, for both complexes[20].

Even though the number of iron ions in compounds 7 and 8 exceed 10, no magnetic hyperfine interactions indicating the presence of collective magnetic correlations among iron spins are observed in the Mössbauer spectra. This is due to the fact that the Fe-Fe exchange interactions present in both of these molecules are of lower dimensionality. No magnetic exchange pathways exist to cross link rings in 8 and thus this cluster remains of lower magnetic dimensionality even though topologically it is a three-dimensional structure, unlike 7 which is topologically as well as magnetically lower dimensional. Any short-range magnetic correlations, if sustainable by these structures, must have a relaxation frequency $\nu >> \nu_L$, the Larmor precession frequency of the Fe^{57} nucleus, which is of the order of 10^8 sec^{-1}

V. Conclusion

Mössbauer spectroscopy with a short characteristic measuring time of $\sim 10^{-8}$ sec has provided experimental evidence of the presence of intramolecular short-range magnetic order within the $[Fe_{11}]$, $[Fe_{12}]$, $[Fe_{16}Mn]$ and $[Fe_{17}]$ cores of compounds 2, 3, 4, 5, and 6 with a 3-D magnetic exchange interaction network among iron spins. Owing to the extremely small size of the magnetic domain of these compounds, about 10 Å in diameter, superparamagnetic relaxation phenomena dominate the Mössbauer spectral behavior. These systems have provided the first experimental confirmation, to the author's knowledge, of the onset of collective magnetic phenomena associated with the solid-state in molecular systems of nanometer-size containing a number of interacting spins of the order of 10, as initially predicted by theoretical studies in metallic clusters[7]. Furthermore, the observation of hysteresis for the $[Fe_{12}]$ cluster of compound 4 marks the first observation of hysteretic phenomena in a molecular cluster of nanometer-size.

In contrast, no evidence of collective magnetic correlation effects were observed in the magnetically lower-dimensional systems $[Fe_{10}]$, $[Fe_{18}S_{30}]$ or $[Fe_{20}Se_{38}]$. This, however, does not necessarily disprove theoretical predictions that finite antiferromagnetic chains or rings ought to exhibit magnetic correlation effects and be able to sustain spin-wave spectra approximating those of the infinite chain as discussed in the introduction[24]. Rather, it points to the need of an even faster spectroscopic tool, such as neutron scattering and/or even lower sample temperatures in order to probe further magnetic correlations in these systems.

Acknowledgements

The generous contribution of compounds 1, 2, 3, 4, 5, and 6 by S.J. Lippard of MIT and compounds 7 and 8 by R.H. Holm of Harvard University and associated crystallographic data are gratefully acknowledged. The author wishes to thank S. Gorun, W. Micklitz, R.L. Rardin, K. Taft, J.F. You, B. Snyder and S.B. Yu for numerous discussions on the synthesis and x-ray structural characterization of these compounds. The high field magnetization measurements were performed with the assistance of S. Foner and E.J. McNiff of the Francis Bitter National Magnet Laboratory high field users' facility. This work was supported by the Office of Naval Research

VI. References

[1] J.R. Anderson, **Structure of Metallic Catalysts** (Academic Press, New York, 1975); J.H. Sinfelt, in *Annual Review of Materials Science,* edited by R.A. Higgins, R.H. Bube, and R.W. Roberts, (Annual Reviews, Palo Alto, CA, 1972); E.L. Meutterties, T.N. Rhodin, E. Band, C.F. Brucker, and W.R. Pretzer, *Chem. Rev.* **79,** 91 (1979); **The Physical Basis of Heterogeneous Catalysis,** edited by E. Drauglis and R.J. Jaffee (Plenum Publ. Corp., New York, 1975).

[2] K. Bittler and W. Ostertag, *Agew. Chem. Int. Ed. Engl.* **19,** 190 (1980).

[3] P. Ball and L. Garwin, *Nature* **355,** 761 (1992); G.D. Stucky and J.E. MacDougall, *Science* **247,** 669 (1990) and references therein.

[4] J. Demuynch, M.M. Rhomer, A. Stich, and A. Veillard, *J. Chem. Phys.* **75,**3443 (1981); R.C. Baetzold and R.E. Mack, *ibid.* **62,** 1513 (1975), K. Lee, J. Calloway, and S. Dhar, *Phys. Rev.* **B30,** 1724 (1984).

[5] M.G. Mason, *Phys. Rev.* **B27,** 748 (1983) and references therein; S. Raaen and M. Strongin, *ibid.* **32,** 4289 (1985); C. Brechignac, M. Boyer, Ph. Cahuzac, G. Delacretaz, P. Labastie, J.P. Wolf, and L. Wöste, *Phys. Rev. Lett.* **60,** 275 (1988); W. Eberhardt, P. Fayet, D.M. Cox, Z. Fu, A. Kaldor, R. Sherwood, and D. Sondericker, *Phys. Rev. Lett.* **64,** 780 (1990); K.E. Schriver, J.L. Persson, E.C. Honea, and R.L. Whetten, *ibid.* **64,** 2539 (1990); K.D. Kolenbrander and M.L. Mandich, *ibid.* **65,** 2169 (1990).

[6] R.P. Messmer, S.K. Knudson, K.H. Johnson, J.B. Diamond, and C.Y. Yang, *Phys. Rev.* **B13,** 1396 (1976).

[7] C.Y. Yang, K.H. Johnson, D.R. Salabub, K. Kaspar, and R.P. Messmer, *Phys. Rev.* **B24,** 5673 (1981).

[8] G.C. Shull and H.A. Mook, *Phys. Rev. Lett.* **16,** 184 (1966).

[9] W.A. de He , P. Milani, and A. Chatelain, *Phys. Rev. Lett.* **65,** 488 (1990); **Elemental and Molecular Clusters,** edited by G. Benedek, T.P. Martin, and G. Pacchioni (Springer, Berlin, 1988); J.J. Krebs, P. Lubitz, A. Chaiken, and G.A. Prinz, *Phys. Rev. Lett.* **63,** 1645 (1989); B. Heinrich, Z. Celinski, J.F. Cochran, W.B. Muir, J. Rudo, Q.M. Zhong, S. Arrott and K. Myrtle, *Phys. Rev. Lett.* **64,** 673 (1990); **Microclusters,** edited by S. Sugano, Y. Nishina, and S. Ohnishi, (Springer, Berlin, 1987); E.S. Smotkin et.al., *Chem. Phys. Lett.* **152,** 265 (1988); M.L. Steigerwald and E.L. Brus, *Annu. Rev. Mater. Sci.* **19,** 471 (1989).

[10] O. Cheshnovsky, K.J. Taylor, J. Conceicao, and R.E. Smalley, *Phys. Rev. Lett.* **64,** 1785 (1990).

[11] A.M.Thayer, M.L. Steigerwald, T.M. Duncan, and D.C. Douglan, *ibid.* **60,** 2673 (1988).

[12] D.M. Cox, D.J. Trevor, R.L. Whetten, E.A. Rohlfing, and A. Kaldor, *Phys. Rev.* **B32,** 7290 (1985); J. Merikoski, J. Timonen, M. Manninen, and P. Jena, *Phys. Rev. Lett.* **66,** 938 (1991) and references therein; J.P. Bucher, D.C. Douglass nd L.A. Bloomfield, *Phys. Rev. Lett.* **66,** 3052 (1991).

[13] S.M. Gorun and S.J. Lippard, *Nature* **319,** 666 (1986).

[14] S.M. Gorun, G.C. Papaefthymiou, R.B. Frankel, and S.J. Lippard, *J. Am. Chem. Soc.* **109,** 3337 (1987).

[15] W. Micklitz and S.J. Lippard, *J. Am. Chem. Soc.* **111,** 6856 (1989).

[16] G. Schmid, *Polyhedron* **7,** 2321 (1988); A. Ceriotti, F. Demartin, G. Langoni, M. Manassero, M. Marchionna, G. Pira, and M. Sansoni, *Angew. Chem. Int.* Ed. Engl. **24,** 697 (1985).

[17] J.F. You, B.S. Snyder, G.C. Papaefthymiou, and R.H. Holm, *J. Am. Chem. Soc.* **112,** 1067 (1990) and references cited therein.

[18] K.L. Taft and S.J. Lippard, *J. Am. Chem. Soc.* **112,** 9629 (1990).

[19] J.F. You and R.H. Holm, Inorg. Chem. **30,** 1431 (1991).

[20] J.F. You, G.C. Papaefthymiou and R.H. Holm, J. Am. Chem. Soc. **114,** 2697 (1992).

[21] G.C. Papaefthymiou in **Clusters and Cluster-Assembled Materials,** edited by R.S. Averback, J. Bernholc, and D.L. Nelson, MRS Symposium Proceedings, Vol. 206 (Materials Research Society, Pittsburgh, 1991), p.539.

[22] L.J. de Jongh and A.R. Miedema, *Adv. Phys.* **23,** 1 (1974).

[23] J. Van Kranendouk and J.H. Van Vleck, *Rev. Mod. Phys.* **30,** 1 (1958).

[24] J. des Cloizeaux and J.J. Pearson, *Phys. Rev.* **128,** 2131 (1962.

[25] J.C. Bonner and M. E. Fisher, *Phys. Rev.* **135,** A640 (1964).

[26] F. Liu, S.N. Khanna and P. Jena, *Phys. Rev. B* **42,** 976 (1990); F. Liu, M.R. Press, S.N. Khanna and P. Jena *ibid.* **39,** 6914 (1989).

[27] W.F. Brown, Jr., *J. Appl. Phys.* **30(4)** (Suppl.), 1305 (1959).

[28] D.G. Rancourt, *Hyp. Int.* **40,** 183 (1988).

[29] M.F. Thomas, *"Mössbauer Spectroscopy on Low Dimensional Magnetic Solids"*, in **Mössbauer Spectroscopy Applied to Inorganic Chemistry,** Vol. 2, edited by Gary J. Long (Plenum Publ. Corp., 1987) p.209.

[30] T.G. Spiro, S.E. Allerton, J. Denner, A. Terzis, R. Bils, and P. Saltman, *J. Am. Chem. Soc.* **88,** 2721 (1966); B.A. Sommer, D.W. Margerum, J. Reuner, P. Saltman, and T.G. Spiro, *Bioinorg. Chem.* **2,** 295 (1973).

[31] S.M. Gorun, in **Metal Clusters in Proteins,** L. Que, Jr., Editor (American Chemical Society, Washington, DC, 1988), Ch. 10, p.196 and references cited therein; S.J. Lippard, *Angew. Chem. Int.*, Ed. Engl. **27,** 344 (1988) and references cited therein.

[32] E.C. Theil, *Annu. Rev. Biochem.* **56,** 289 (1987).

[33] S.H. Yang,C.L. Pettiette, J. Conceicao, O. Cheshnovsky and R.E. Smalley, *Chem. Phys. Lett.* **139,** 233 (1987); W. Krätschmer, L.D. Lamb, K. Fostiropoulos, and D.R. Huffman, *Nature,* **347,** 354 (1990).

[34] B. Blume, *Phys. Rev. Lett.* **18,** 305 (1967).

[35] J. Chappert, *J. de Phys.* **C6,** 71 (1974); J. Chappert, J. Teillet, and F. Varret, *J. Magn. Magn. Mater.* **11,** 200 (1979).

[36] J.M.D. Coey, *Phys. Rev. Lett.* **27,** 1140 (1971); N.F. Thomas and C.G. Johnson in **Mössbauer Spectroscopy** D.P. E. Dickson and F.T.Berry, editors, (Cambridge Univ. Press, Cambridge 1986) Ch4, p.143; Q.A. Parkhurst, C.E. Johnson and M.F. Thomas, *J. de Phys.***C18,** 3249 (1985); A.E. Berkowitz, J.A. Lahut, I.S. Jacobs, L.M. Levinson and D.W. Forestor, *Phys. Rev. Lett* **.34,** 594 (1975).

[37] R.B.Frankel in **Mössbauer Effect Methodology** J. Gruverman, C.W. Siedel and P.K. Dieterly, Editors, Vol. 9, p.151 (1974).

[38] W.H. Armstrong and S.J. Lippard, *J. Am. Chem. Soc.**106,*** 4632 (1984).

[39] A.P. Ginsberg, *Inorg. Chim. Acta. Rev* . **5,** 45 (1971).

[40] L.R.Carlin, **Magnetochemistry** (Springer-Verlag, 1986).

[41] K.S. Murray, *Coord. Chem. Rev.* **12,** 1 (1974); D.M. Kurtz, Jr. *Chem. Rev.* **90,** 585 (1990).

[42] W. Kundig, H. Bömmel, G. Constabaris, and R.H. Linquist, *Phys. Rev.* **142,** 327 (1966); K.S. Kaufman, G.C. Papaefthymiou, R.B.Frankel and A. Rosenthal, *Biochim. Biophys. Acta* **629,** 522 (1980),

[43] S. Mørup, H. Topsoe, and J. Lipka, *J. de Phys.* **51,** 6-281 (1976); G.D. Watt, R.B. Frankel, G.C. Papaefthymiou, K. Spartalian, E.I. Stiefel, *Biochemistry* **25,** 4330 (1986).

[44] N.N. Greenwood and T.C. Gibb, **Mössbauer Spectroscopy** (Chapman and Hall, Ltd. London 1971).

[45] C. Kittel, **Introduction to Solid State Physics,** John Wiley & Sons, Inc., New York, London, Sydney (1966); **Solid State Physics,** G. Burns, Academic Press, Inc., New York, London, Toronto (1985).

[46] W.H. Armstrong, A. Spool, G.C. Papaefthymiou, R.B. Frankel, and S.J. Lippard, *J. Am. Chem. Soc.* **106,** 3653 (1984).

[47] J.J. Girerd, G.C. Papaefthymiou, A.D. Watson, E. Gamp, K.S. Hagen, N. Edelstein, R.B. Frankel and R.H.Holm. *J. Am. Chem. Soc.* 106, 5941 (1984). A typical example for a high spin ferric trimer complex Mössbauer spectrum in an external magnetic field is shown in Fig. 6 of this reference. This type of behavior may be taken as the Mössbauer signature of an antiparallel-spin- coupled iron molecular paramagnet.

[48] R.E. Vandenberghe and E. DeGrave in **Mössbauer Spectroscopy Applied to Inorganic Chemistry vol. 3,** p. 59, G.F. Long and F. Grädjean, Editors, Plenum Publ. Corp., New York (1989).

[49] D. Chowdhury, **Spin Glasses and Other Frustrated Systems,** Princeton University Press, Princeton, New Jersey (1986); C.M. Hurd, *Contem. Phys.* **23,** 469 (1982).

[50] The dipole-dipole interaction energy $\mu_1 \cdot \mu_2 / r^3 \sim 10^{-20}$ ergs for two magnetic dipoles of 1 μ_B each separated by a distance r = 20Å, which is much weaker than either thermal energies, kT, for the lowest temperature used in these experiments, or the orientation energy of each dipole $-\mu \cdot H_o$ in the external field of 80 KOe, both of which are of the order of 10^{-16} ergs.

VII. Figure Captions

Fig. 1. Comparison of the occupied SCF-Xα-SW electronic energy levels for Cu_2, Cu_8, and Cu_{13} with the electronic density of states for bulk crystalline copper calculated by SCF-Xα–KKR band-structure theory. For the sake of comparison, the latter has been adjusted so that the Fermi levels of the crystal and Cu_{13} cluster approximately coincide. Also shown for comparison are the SCF-Xα energy levels of the isolated Cu atom for two different electronic configurations. From Messmer et al. ref. 6.

Fig. 2. (a) Representation of the magnetization density for bulk iron in a [100] plane measured by neutron scattering. Adapted from ref. 8. The positive (circular) contours have been drawn schematically in order to emphasize the (hatched) region of negative polarization. The symbols represent the following values of the magnetic field: o, + 1.0 ± 0.3 kG; •, -1.0 ± 0.3 kG; Δ, -2.0 ± 0.4 kG. (b) Contour map of the spin density for Fe_{15} plotted in a [100] plane containing four atoms. Dashed lines represent negative values of the spin density. The lowest contour has the value 0.001 a.u. (0.524 kG) and adjacent contours differ by a factor of 2. From ref. 7

Fig. 3. Ultraviolet photoemission spectroscopy of negative copper clusters in the 1-410-atom size range mass selected from a supersonic cluster beam, taken with an F_2 excimer laser at 7.9 eV. From ref. 10.

Fig. 4. ^{77}Se NMR spectra of three sizes of CdSe-R (R = phenyl, butyl) clusters in pyridine, and bulk cubic CdSe. The spectra are plotted on the σ scale for chemical shifts with negative shifts corresponding to lower field. With increasing particle size, the relative proportions of the three-line shape components change. For the largest size cluster, the intensity is shifted almost entirely towards the chemical shift of the bulk material, shown at the bottom. From ref. 11.

Fig. 5. Discrete points depict the results of theoretical calculations of the spin-wave spectra of the antiferromagnetic Heisenberg exchange Hamiltonian with periodic boundary conditions for a linear chain of N spins. The solid lines indicate the spectrum of the infinite chain. From ref. 24.

Fig. 6. Crystal structure of $Fe_{11}O_6(OH)_6(O_2CPh)_{15}\cdot 6THF$ (1) showing 40% probability thermal ellipsoids. Only 7 of the 11 Fe ions are discernible in this view of the molecule.

Fig. 7. Crystal structure of $Fe_{16}MnO_{10}(OH)_{10}(O_2CPh)_{20}$ (2) showing 20% probability thermal ellipsoids. Only 15 of the 16 Fe atoms are discernible.

Fig. 8. Crystal packing of Fe_{11} clusters. Only the inner magnetic cores $[Fe_{11}\ O_6(OH)_6]^{15+}$ of the clusters are shown. Unit cell: a=28.5Å, b=18.6Å, c=29.9Å, α=90°, β=115.9°, γ=90°. Average distance between cluster centroids ~20Å.

Fig. 9. Formal construction of the $Fe_{16}Mn$ cluster and extended structures by the fusion of twisted pentacapped trigonal prisms of the Fe_{11} cluster.

Fig. 10. Basic steps of the synthesis and crystallographic structure of $Li_2[Fe_{12}(O)_2(OMe)(OAc)_{10}(MeOH)_2]$ (3) The two central iron ions are in the ferric state (as indicated) with all other being in the ferrous state.

Fig. 11. Depiction of polymerization of compound (3) in the crystal lattice.

Fig. 12. Basic steps in the synthesis and crystallographic structure of $[Fe_{12}(O)_2(OCH_3)_{18}(O_2CCH_3)_6(CH_3OH)_4]$(4). The four ferric ions are shown. All others are ferrous

Fig. 13. (a)RTP drawng of the planar projection of $[Fe(OMe)_2(O_2CCH_2Cl)]_{10}$ with 50% probability thermal ellipsoids and atom labels; primed and unprimed atoms are related by a center of inversion, chlorine and hydrogen atoms are omitted for clarity. The Fe...Fe distance for adjacent iron averages 3.028 Å..(b) Drawing of side-on view. From ref. 18.

Fig. 14. Schematic representation of the buildup of core units of clusters by connection of Fe_2S_2 rhombs (1) by edge-sharing (2), Fe vertex-sharing (3), and S vertex-sharing (4). Structures 5-13 are developed by additional connectivity modes of these types.

Fig. 15. (a) Structure of $[Na_2Fe_{18}S_{30}]^{8-}$ showing 50% probability ellipsoids. Primed and unprimed atoms are related by an inverse center. (b) Side-on view of the molecule.

Fig. 16. Stacking of the $Fe_{18}S_{30}$ rings in the crystal. There is an approximately 20 Å distance between the centroids of the adjacent rings.

Fig. 17. (a) Structure of $[Na_9Fe_{18}S_{30}]^{9-}$. Primed and unprimed atoms are related by an imposed C_2 axis passing through Na(0) and perpendicular to the $Fe_2(3,3')Se_2(6.6')$ rhomb. (b) Depiction of the pseudo-C_3 axis along the Fe(10)-Fe(10') vector.

Fig. 18. Effective moment for the $[Fe_{11}]$ cluster vs temperature.

Fig. 19. Temperature-dependent molar susceptibility (o) and effective moment (•) plot for the $[Fe_{16}Mn]$ cluster at 5 kG.

Fig. 20. Temperature-dependent molar susceptibility (o) and effective momen (•) plot for the $[Fe_{17}Mn]$ cluster at 5 kG.

Fig. 21. High field magnetization study for $[Fe_{11}]$ at 1.5 K.

Fig. 22. Results of a high field magnetization study for $[Fe_{16}Mn]$ at 1.48 K.

Fig. 23. Results of a high field magnetization study for $[Fe_{17}]$ at 1.5 K.

Fig. 24. Mössbauer spectra of polycrystalline $[Fe_{11}O_6(OH)_6(O_2CPh)_{15}]$.6THF at various temperatures.

Fig. 25. Mössbauer spectra of polycrystalline $[Fe_{16}MnO_{10}(OH)_{10}(O_2CPh)_{20}]$ at various temperatures.
Fig. 26. Mössbauer spectra of polycrystalline $[Fe_{17}O_{10}(OH)_{10}O_2CPh)_{20}]$ at various temperatures.

Fig. 27. (a) Low temperature Mössbauer spectra of 2 in external magnetic fields, H_o, parallel to the γ-ray direction. The solid line is a least-square fit of the experimental data to a distribution of internal magnetic fields. (b) The resulting distribution of internal magnetic fields at the sites of the iron nuclei.

Fig. 28. (a) Low temperature Mössbauer spectra of 5 in the absence and presence of a longitudical external magnetic field, H_o. The solid line is a least-square fit of the experimental data to a distribution of internal magnetic fields. (b) The resulting distribution of internal magnetic fields at the sites of the iron nuclei.

Fig. 29. (a) Low temperature Mössbauer spectra of 6 in the absence and presence of a longitudical external magnetic field, H_o. The solid line is a least-square fit of the experimental data to a distribution of internal magnetic fields. (b) The resulting distribution of internal magnetic fields at the sites of the iron nuclei.

Fig. 30. Temperature-dependent Mössbauer spectra of
$[Fe_{12}(O)_2(OCH_3)_{14}(O_2CCH_3)_{10}(CH_3OH)_2]\ Li_2$ (3)

Fig. 31. Temperature-dependent Mössbauer spectra for
$[Fe_{12}(O)_2(OCH_3)_{18}(O_2CCH_3)_6(CH_3OH)_4]$ (4).

Fig. 32. Susceptibility studies for $[Fe_{12}(O)_2(OCH_3)_{18}(O_3CCH_3)_6(CH_3OH)_4]$ (4). Overall paramagnetic behavior is seen. The sharp increase of μ_{eff} with temperature indicates the presence of low-lying higher spin states.

Fig. 33. Onset of hysteretic effects for compound 4 at low temperatures. The traces at 1.4 K and 0.6 K are indistinguishable.

Fig. 34. Mössbauer spectra of the "ferric wheel" $[Fe(OCH_3)_2(O_2CCH_2Cl)]_{10}$(1) at 4.2 K.

Fig. 35. (a) Mössbauer spectra of polycrystalline $(Pr_4N)_6Na_4Fe_{18}S_{30}\cdot 14$ MeCN at T = 4.2 K. The solid line is a least-square fit to the superposition of two quadrupole doublets (see text). (b) Mössbauer spectra of polycrystalline $(Bu_4N)_{4.5}Na_{13.5}Fe_{20}Se_{38}\cdot$ 2PhNH COMe·15EtOH at T = 4.2 K and H_o = 80 KOe parallel to the γ-ray.

VIII. FIGURES

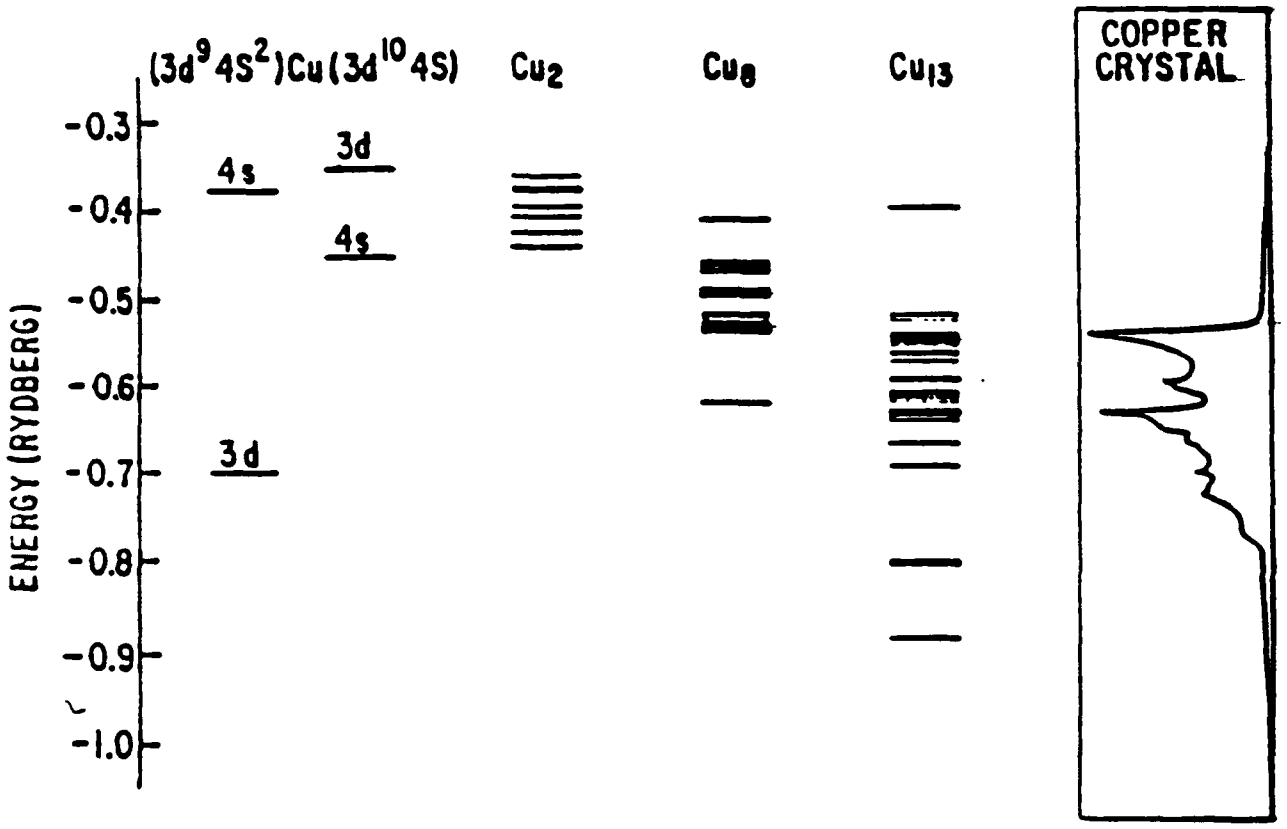

Fig. 1. Comparison of the occupied SCF-Xα-SW electronic energy levels for Cu_2, Cu_8, and Cu_{13} with the electronic density of states for bulk crystalline copper calculated by SCF-Xα–KKR band-structure theory. For the sake of comparison, the latter has been adjusted so that the Fermi levels of the crystal and Cu_{13} cluster approximately coincide. Also shown for comparison are the SCF-Xα energy levels of the isolated Cu atom for two different electronic configurations. From Messmer et al. ref. 6.

Bulk Iron
(neutron diffraction
measurements)

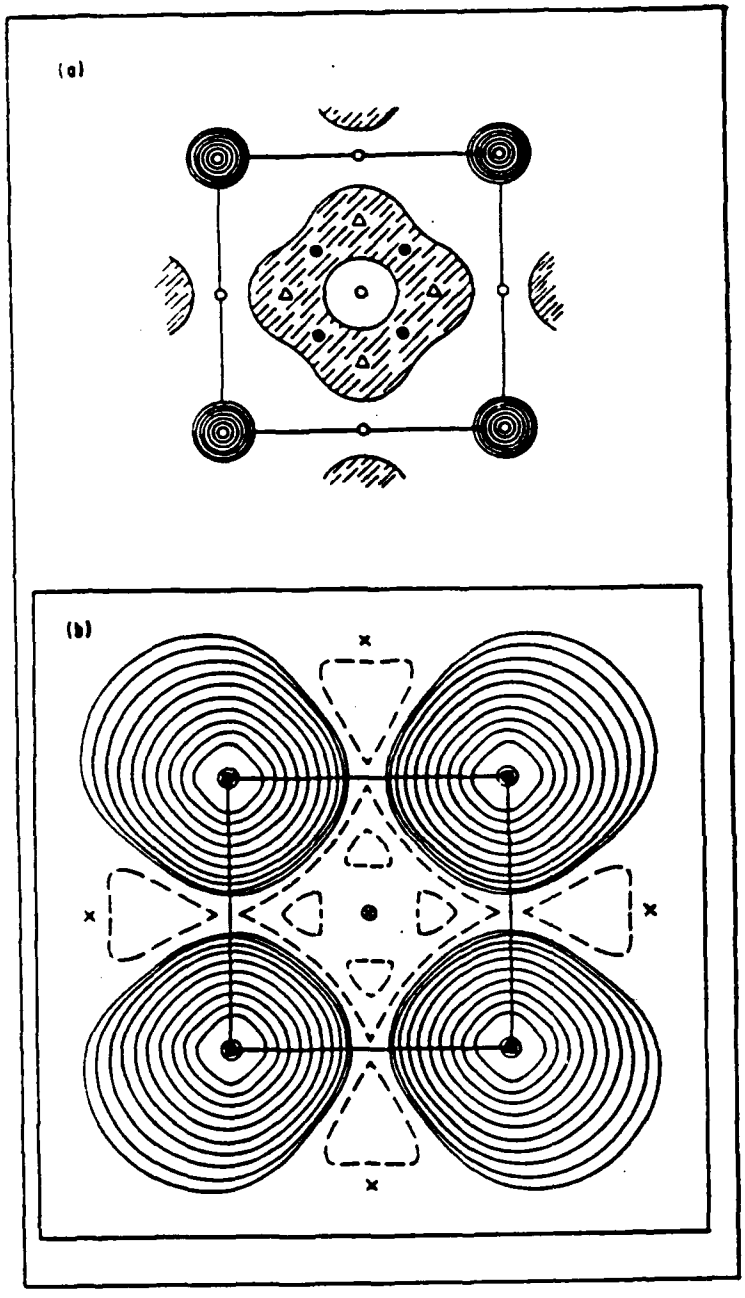

Fe_{15} - cluster
SCF X_α - SW
calculations

Fig. 2. (a) Representation of the magnetization density for bulk iron in a [100] plane measured by neutron scattering. Adapted from ref. 8. The positive (circular) contours have been drawn schematically in order to emphasize the (hatched) region of negative polarization. The symbols represent the following values of the magnetic field: o, + 1.0 ± 0.3 kG; •, -1.0 ± 0.3 kG; Δ, -2.0 ± 0.4 kG. (b) Contour map of the spin density for Fe_{15} plotted in a [100] plane containing four atoms. Dashed lines represent negative values of the spin density. The lowest contour has the value 0.001 a.u. (0.524 kG) and adjacent contours differ by a factor of 2. From ref. 7.

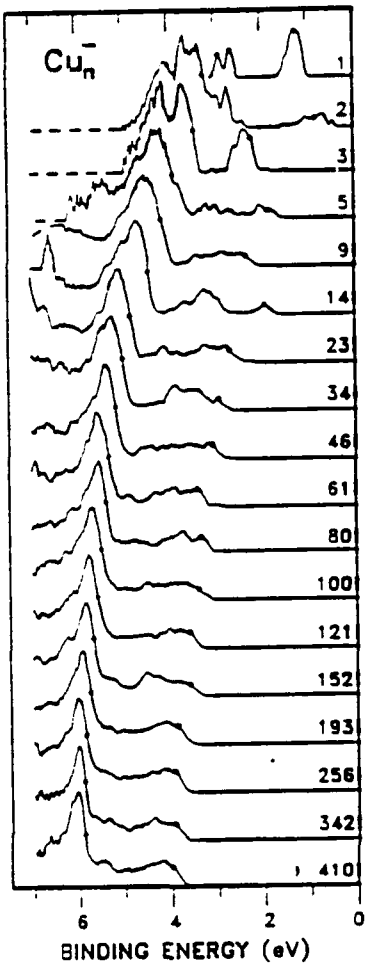

Figure 3: Ultraviolet photoemission spectroscopy of negative copper clusters in the 1–410–atom size range mass selected from a supersonic cluster beam, taken with an F_2 excimer laser at 7.9 eV. From ref. 10.

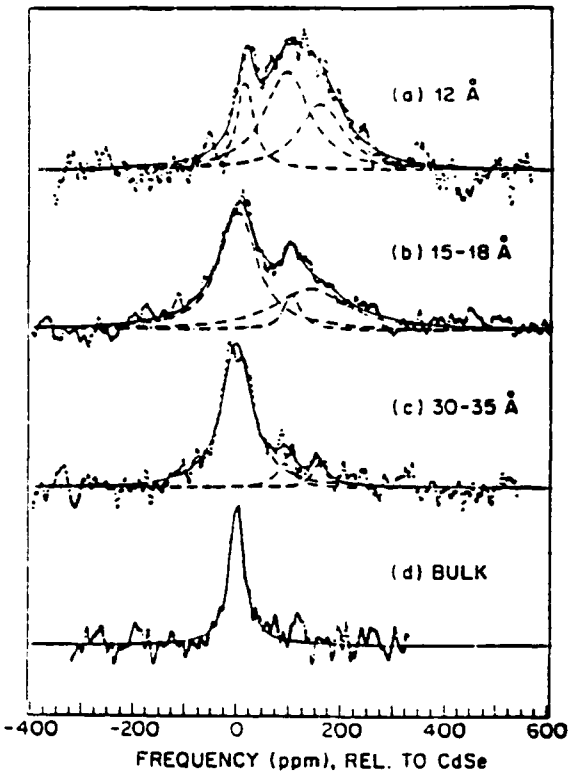

Figure 4: ^{77}Se NMR spectra of three sizes of CdSe–R (R = phenyl, butyl) clusters in pyridine, and bulk cubic CdSe. The spectra are plotted on the σ scale for chemical shifts with negative shifts corresponding to lower field. With increasing particle size, the relative proportions of the three line-shape components change. For thelargest size cluster, the intensity is shifted almost entirely towards the chemical shift of the bulk material, shown at the bottom. From ref. 11.

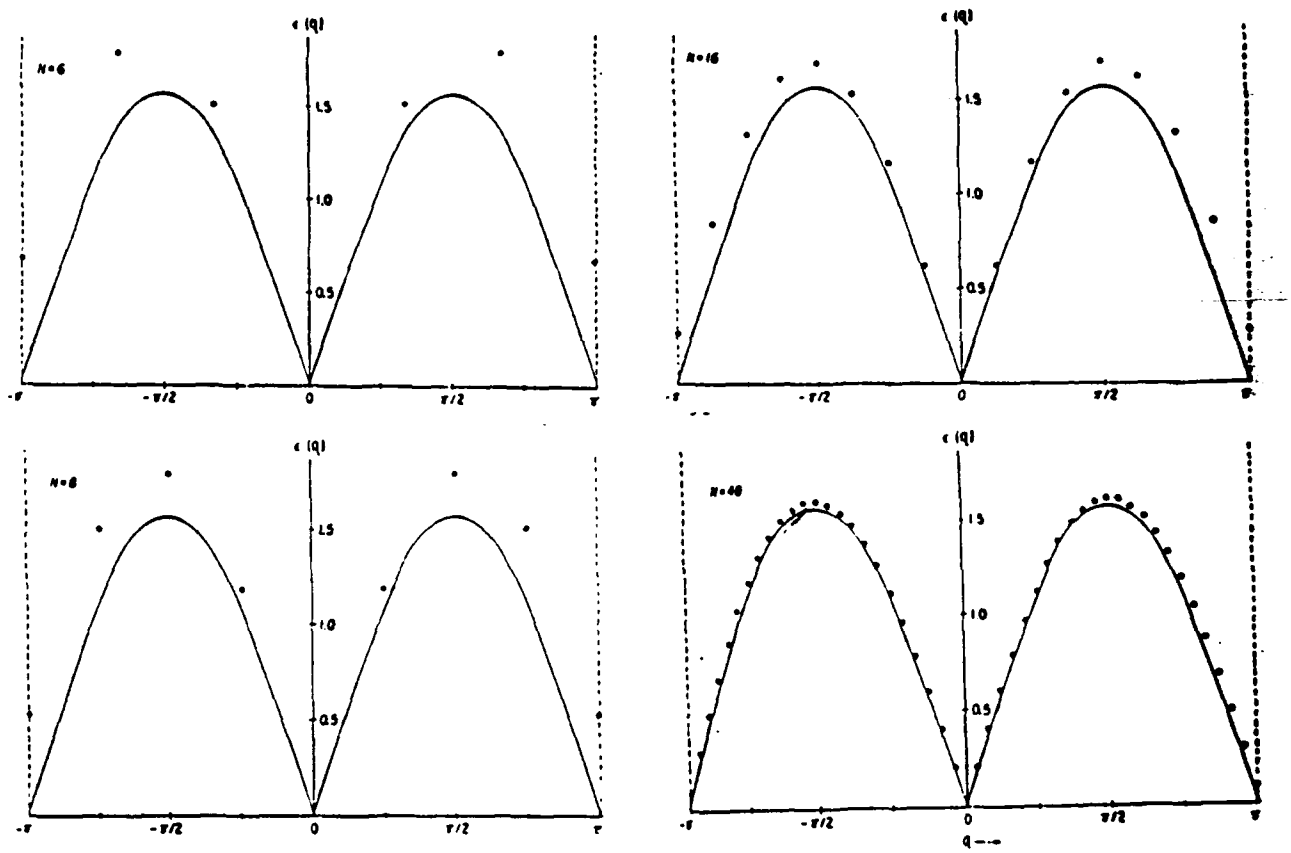

Fig. 5. Discrete points depict the results of theoretical calculations of the spin-wave spectra of the antiferromagnetic Heisenberg exchange Hamiltonian with periodic boundary conditions for a linear chain of N spins. The solid lines indicate the spectrum of the infinite chain. From ref. 24.

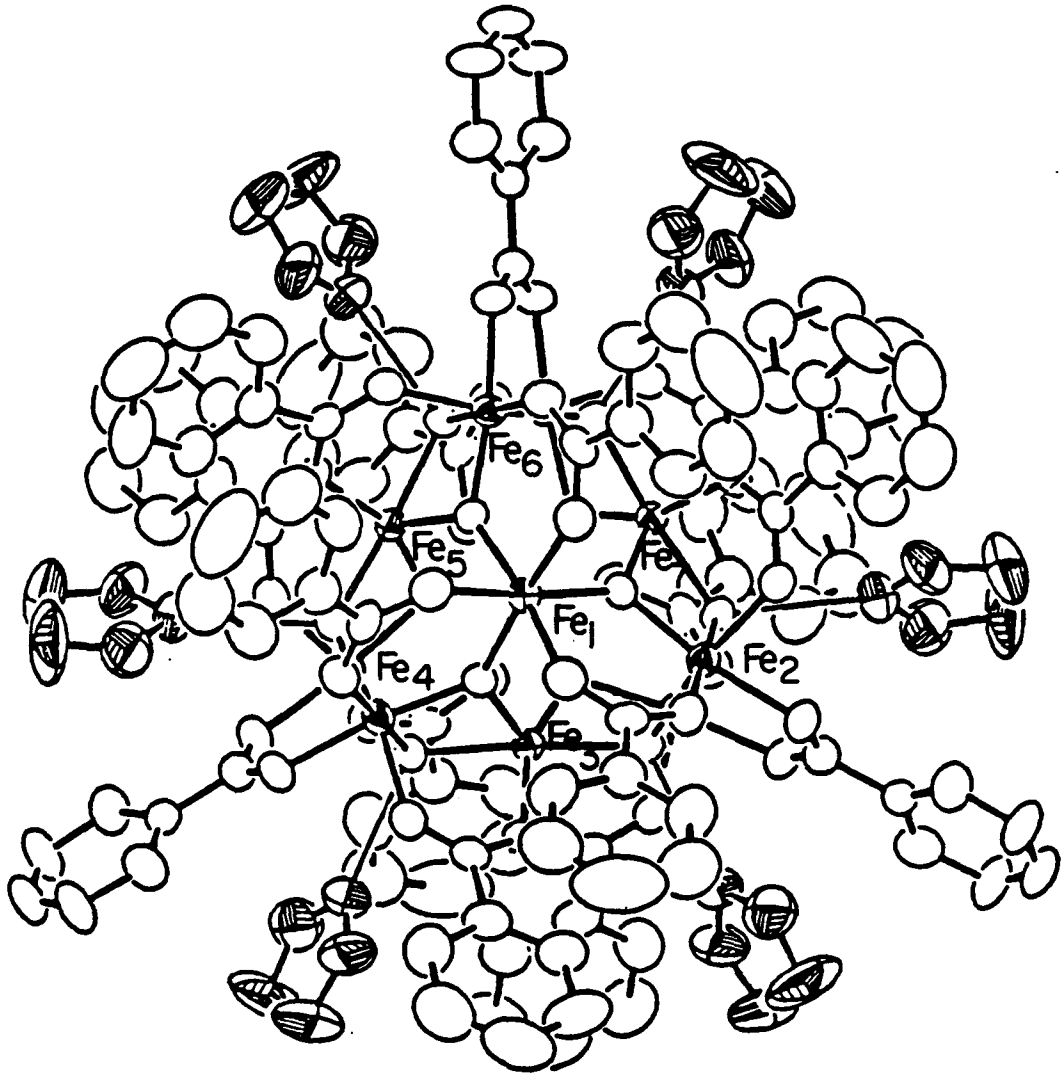

Fig. 6. Crystal structure of $Fe_{11}O_6(OH)_6(O_2CPh)_{15}\cdot 6THF$ (1) showing 40% probability thermal ellipsoids. Only 7 of the 11 Fe ions are discernible in this view of the molecule.

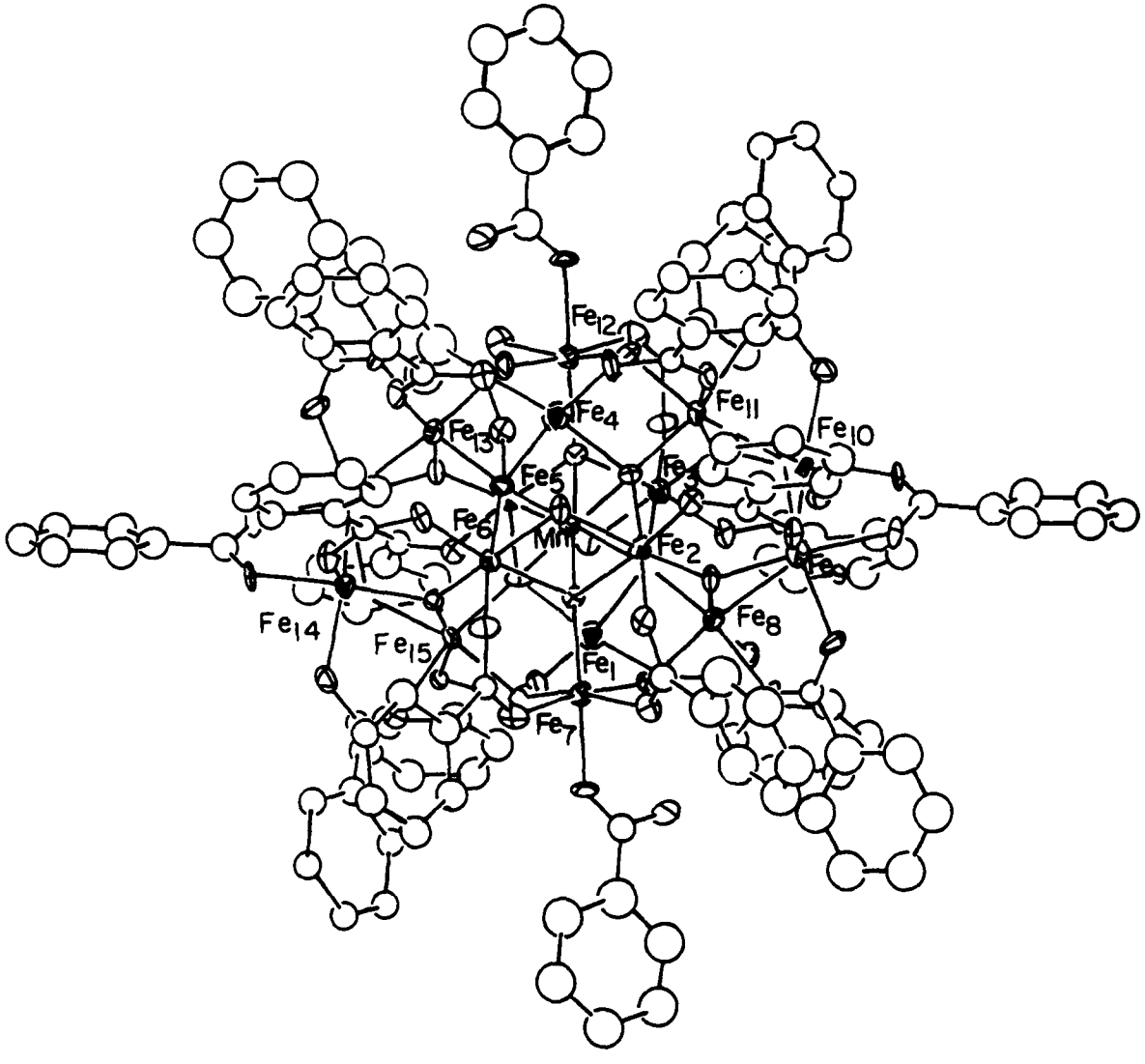

Fig. 7. Crystal structure of $Fe_{16}MnO_{10}(OH)_{10}(O_2CPh)_{20}$ (2) showing 20% probability thermal ellipsoids. Only 15 of the 16 Fe atoms are discernible.

$\{Fe_{11}O_6(OH)_6\}^{15+}$

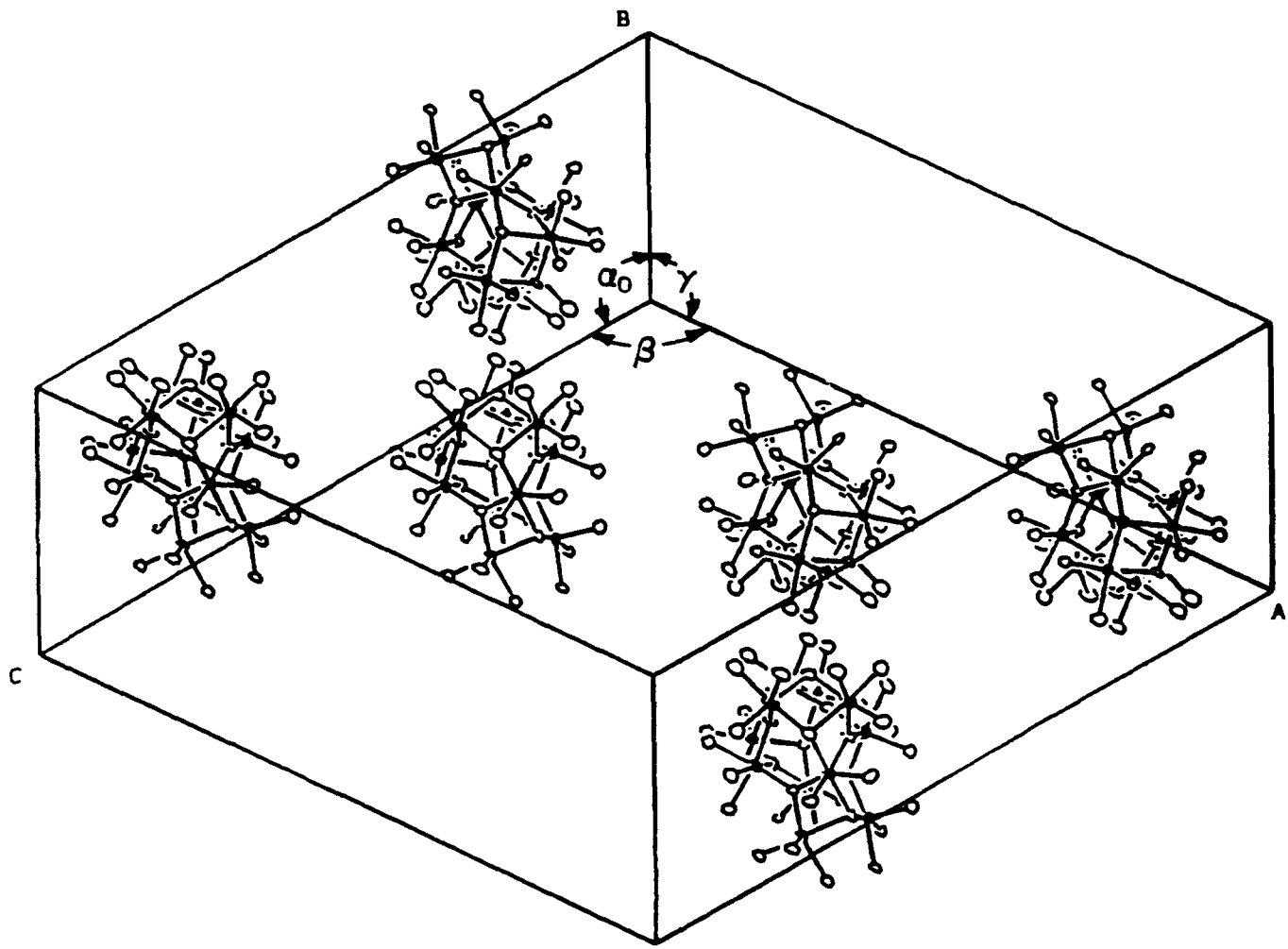

Fig. 8. Crystal packing of Fe_{11} clusters. Only the inner magnetic cores $[Fe_{11}\ O_6(OH)_6]^{15+}$ of the clusters are shown. Unit cell: a=28.5Å, b=18.6Å, c=29.9Å, α=90°, β=115.9°, γ=90°. Average distance between cluster centroids ~20Å.

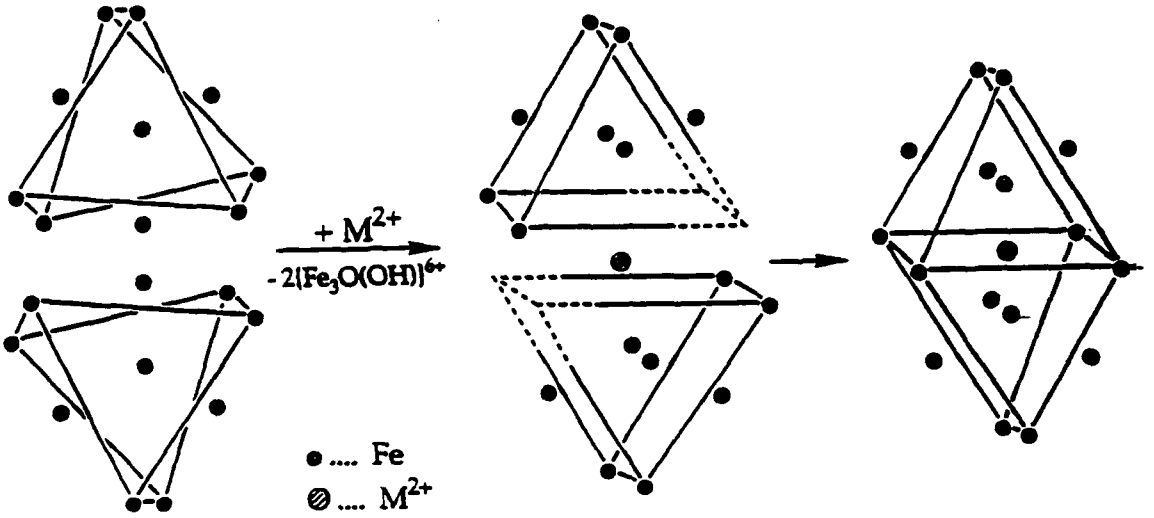

$[M_nFe_{5n+11}O_{4n+6}(OH)_{4n+6}(O_2CPh)_{5n+15}]$, n = 0, 1, 2 etc.

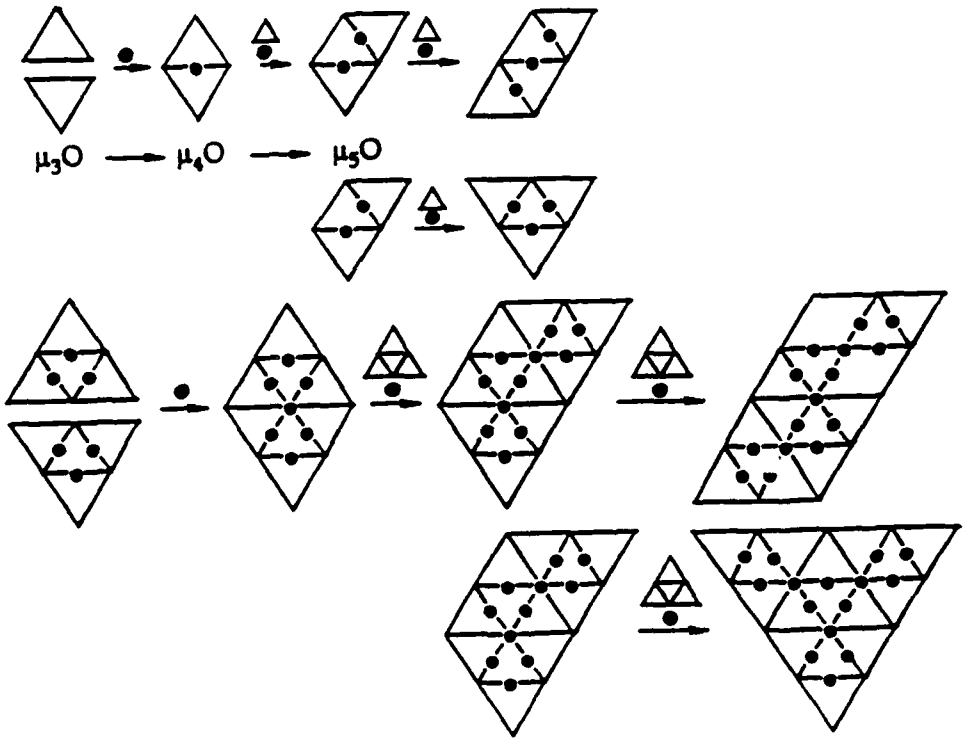

Fig. 9. Formal construction of the $Fe_{16}Mn$ cluster and extended structures by the fusion of twisted pentacapped trigonal prisms of the Fe_{11} cluster.

Synthesis of Polyiron Oxo Complexes from Fe(II) Precursors

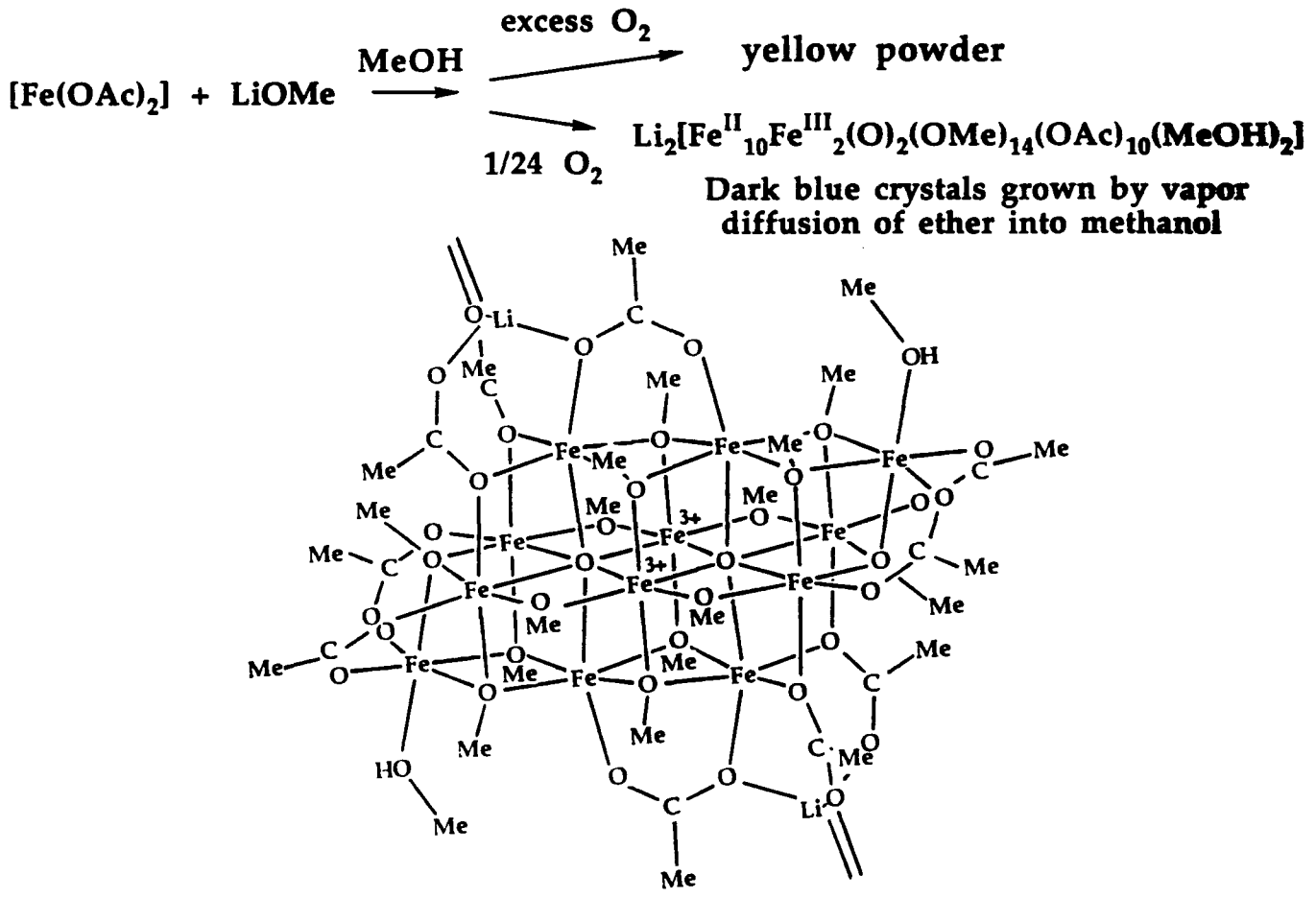

Fig. 10. Basic steps of the synthesis and crystallographic structure of $Li_2[Fe_{12}(O)_2(OMe)(OAc)_{10}(MeOH)_2]$ (3) The two central iron ions are in the ferric state (as indicated) with all other being in the ferrous state.

Repeating Units of $Li_2[Fe^{II}_{10}Fe^{III}_2(O)_2(OMe)_{14}(OAc)_{10}(MeOH)_2]$ in the Crystal Lattice

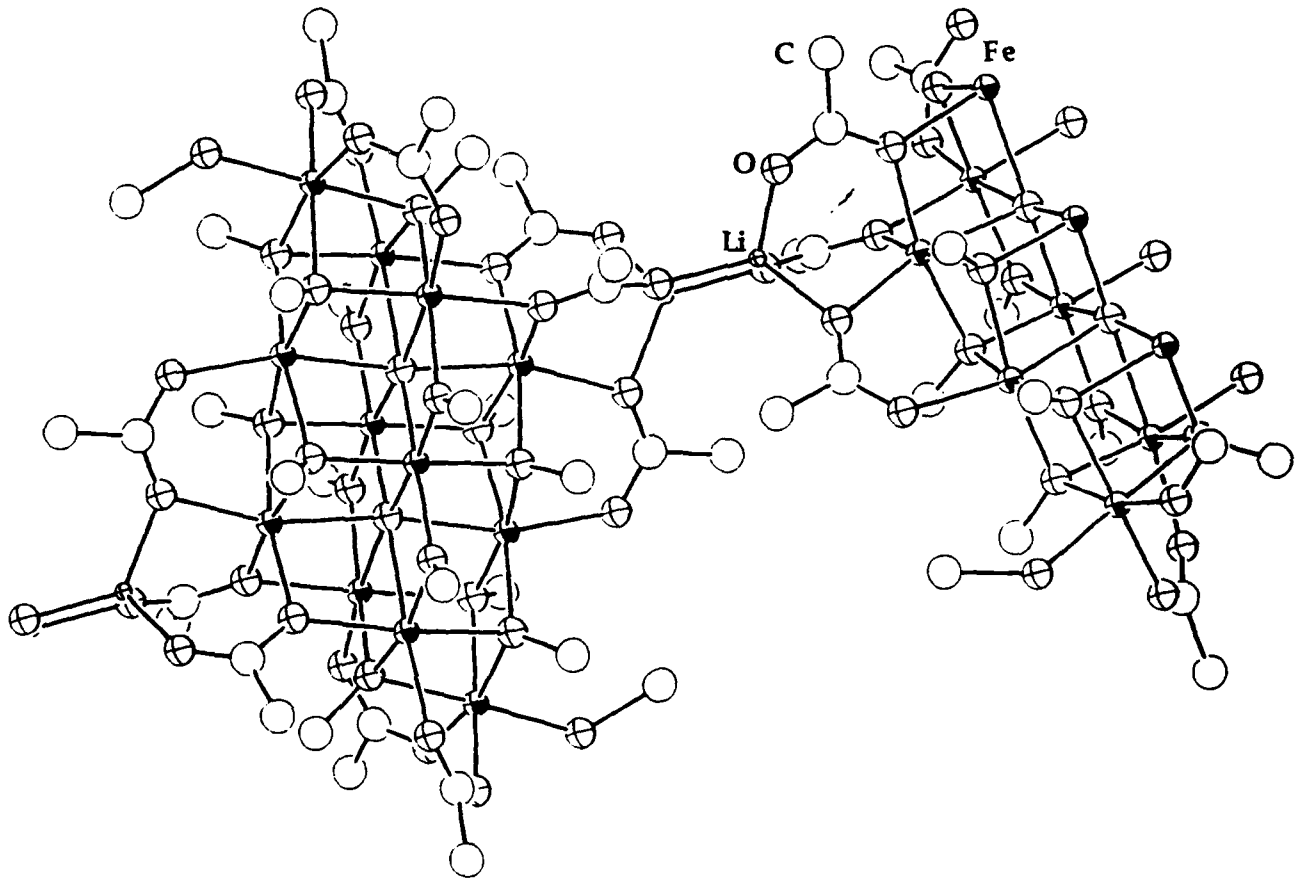

Fig. 11. Depiction of polymerization of compound (3) in the crystal lattice.

Preparation of Polyiron Oxo Complexes from Fe(II) and Dioxygen

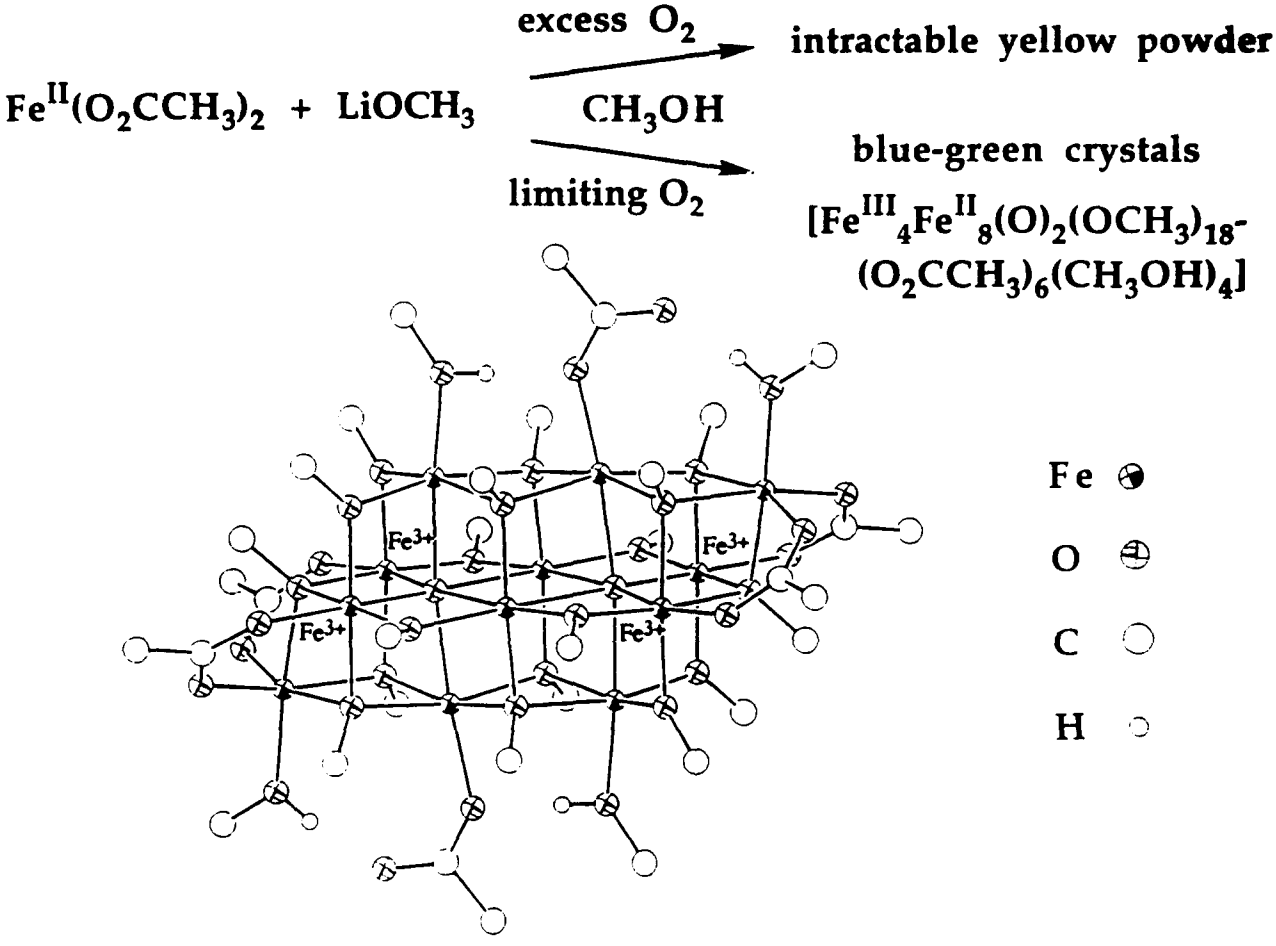

Fig. 12. Basic steps in the synthesis and crystallographic structure of $[Fe_{12}(O)_2(OCH_3)_{18}(O_2CCH_3)_6(CH_3OH)_4]$(4). The four ferric ions are shown. All others are ferrous

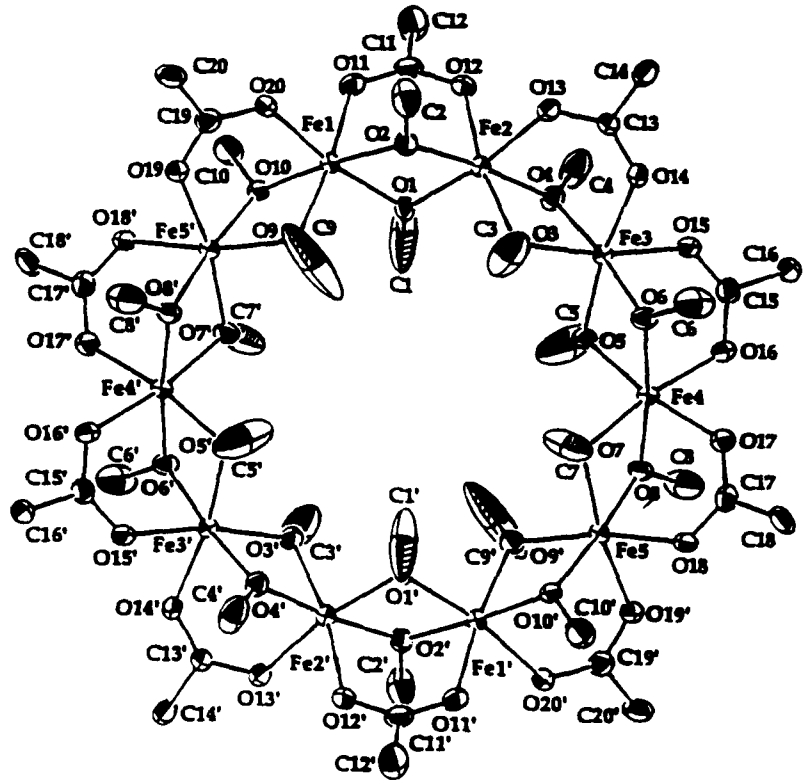

(a)

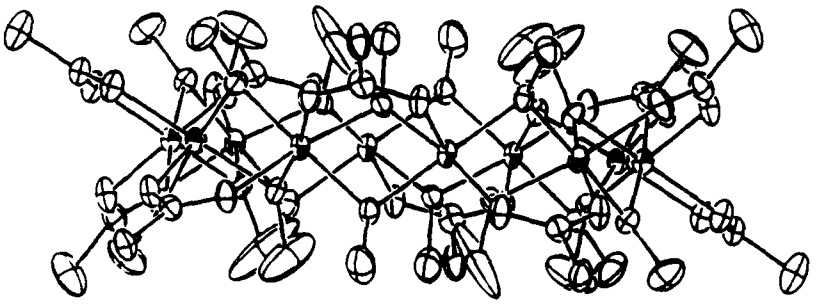

(b)

Fig. 13. (a)RTP drawng of the planar projection of $[Fe(OMe)_2(O_2CCH_2Cl)]_{10}$ with 50% probability thermal ellipsoids and atom labels; primed and unprimed atoms are related by a center of inversion, chlorine and hydrogen atoms are omitted for clarity. The Fe...Fe distance for adjacent iron averages 3.028 Å..(b) Drawing of side-on view. From ref. 18.

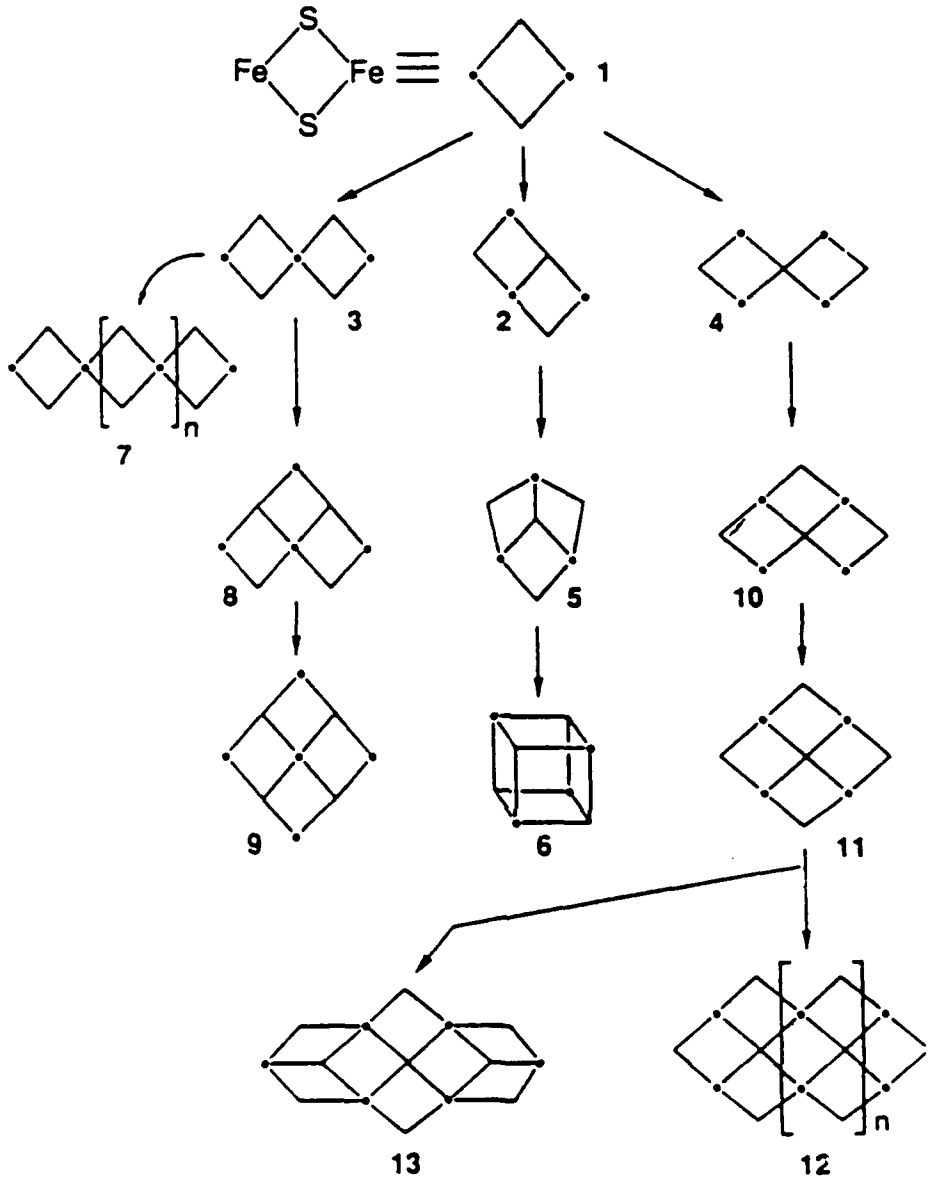

Fig. 14. Schematic representation of the buildup of core units of clusters by connection of Fe_2S_2 rhombs (1) by edge-sharing (2), Fe vertex-sharing (3), and S vertex-sharing (4). Structures 5-13 are developed by additional connectivity modes of these types.

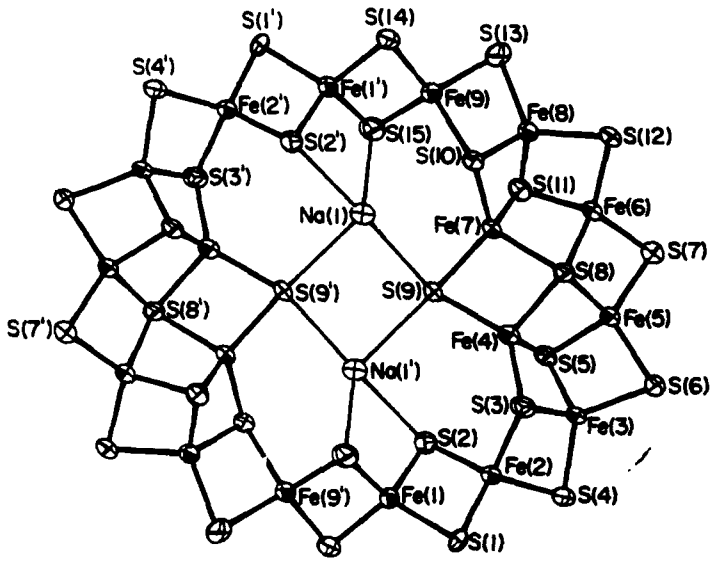

(a)

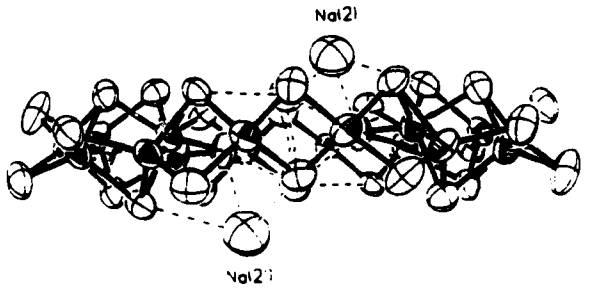

(b)

Fig. 15. (a) Structure of $[Na_2Fe_{18}S_{30}]^{8-}$ showing 50% probability ellipsoids. Primed and unprimed atoms are related by an inverse center. (b) Side-on view of the molecule.

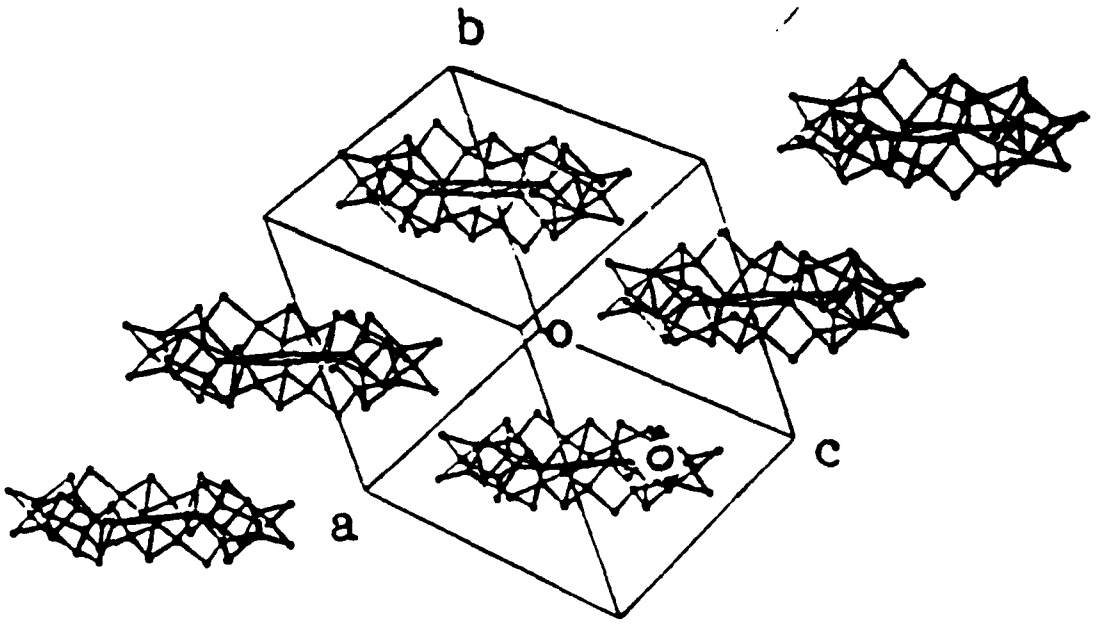

Fig. 16. Stacking of the $Fe_{18}S_{30}$ rings in the crystal. There is an approximately 20 Å distance between the centroids of the adjacent rings.

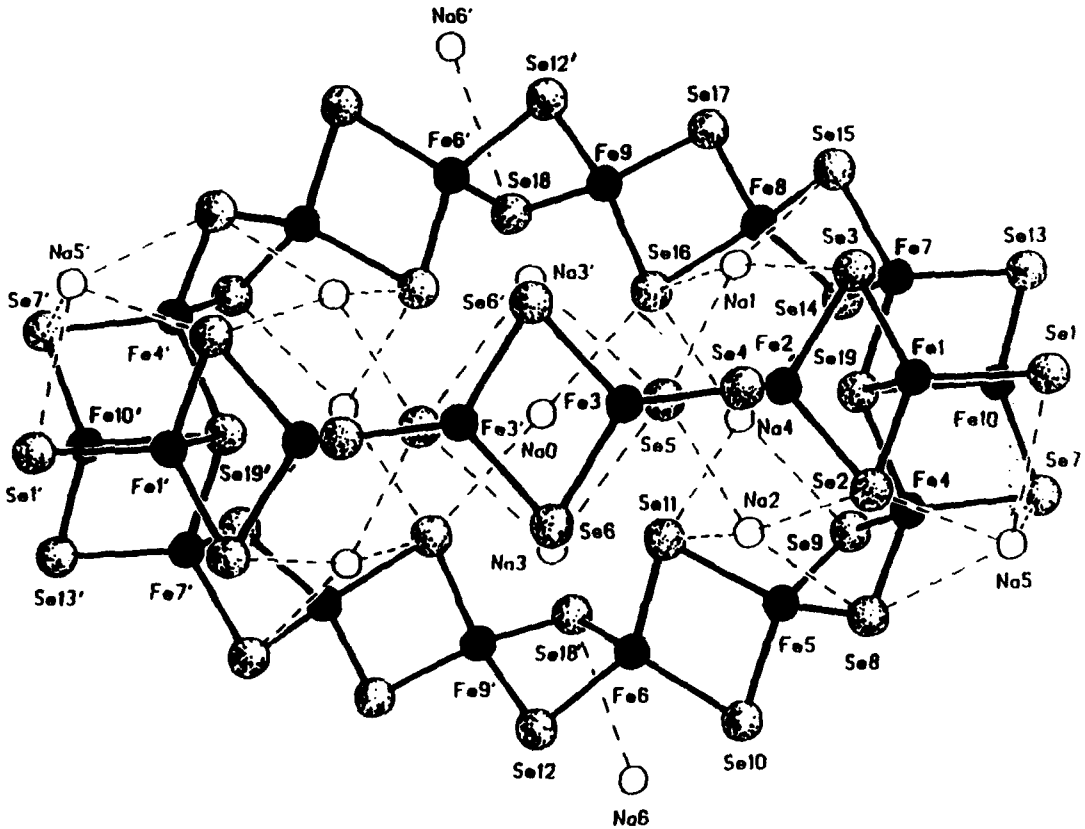

(a)

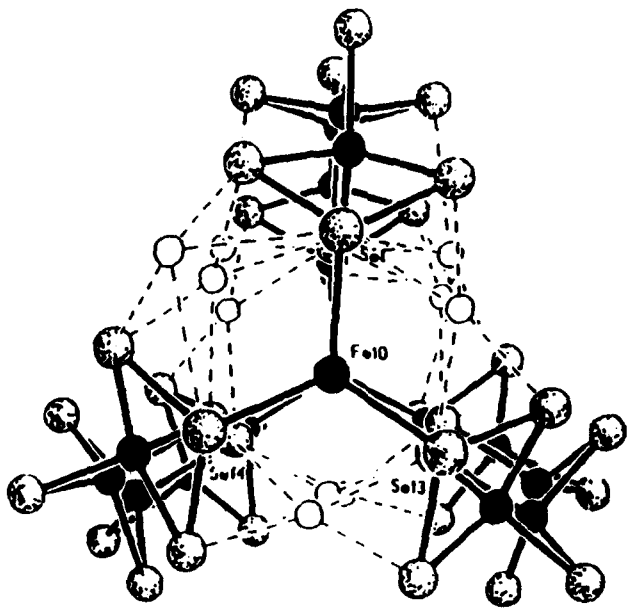

(b)

Fig. 17. (a) Structure of $[Na_9Fe_{18}S_{30}]^{9-}$. Primed and unprimed atoms are related by an imposed C_2 axis passing through Na(0) and perpendicular to the $Fe_2(3,3')Se_2(6,6')$ rhomb. (b) Depiction of the pseudo-C_3 axis along the Fe(10)-Fe(10') vector.

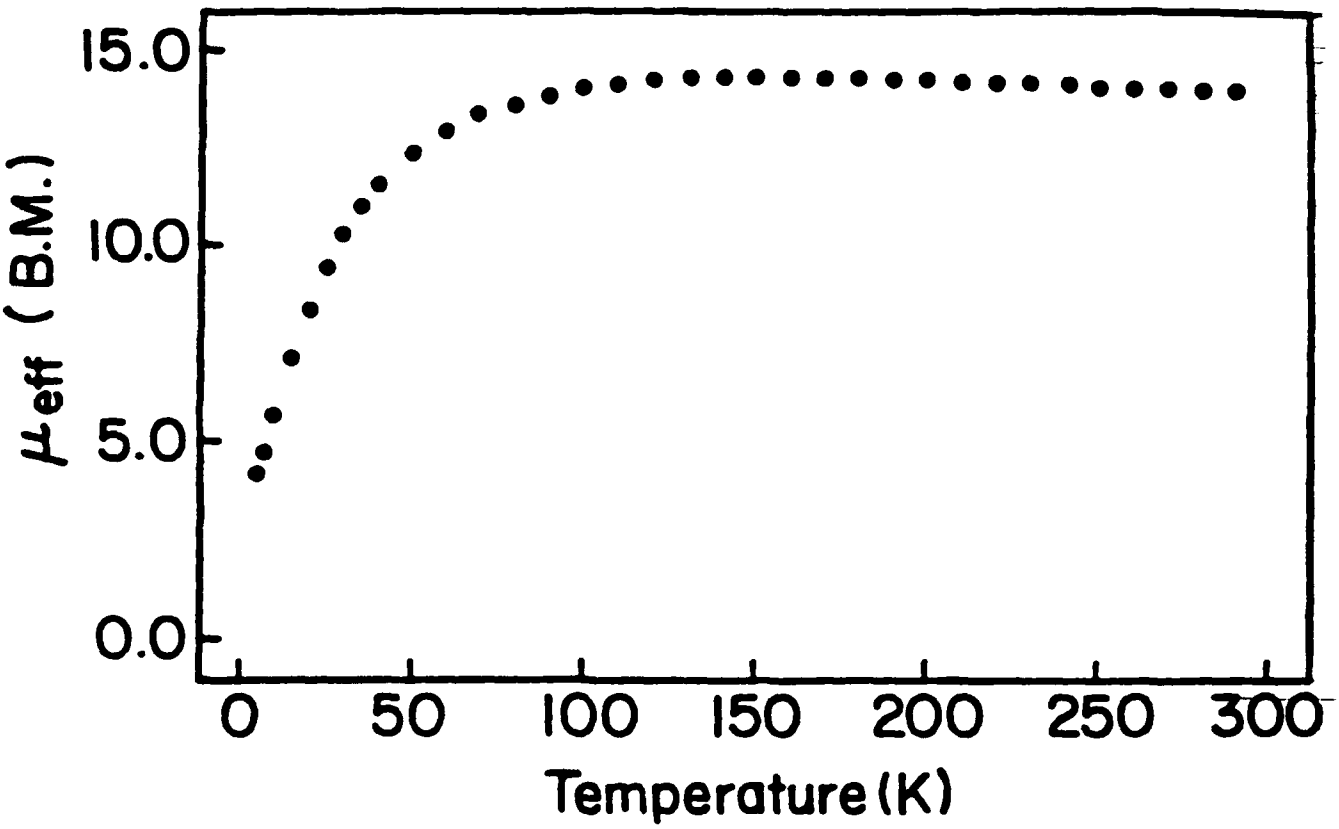

Fig. 18. Effective moment for the [Fe_{11}] cluster vs temperature.

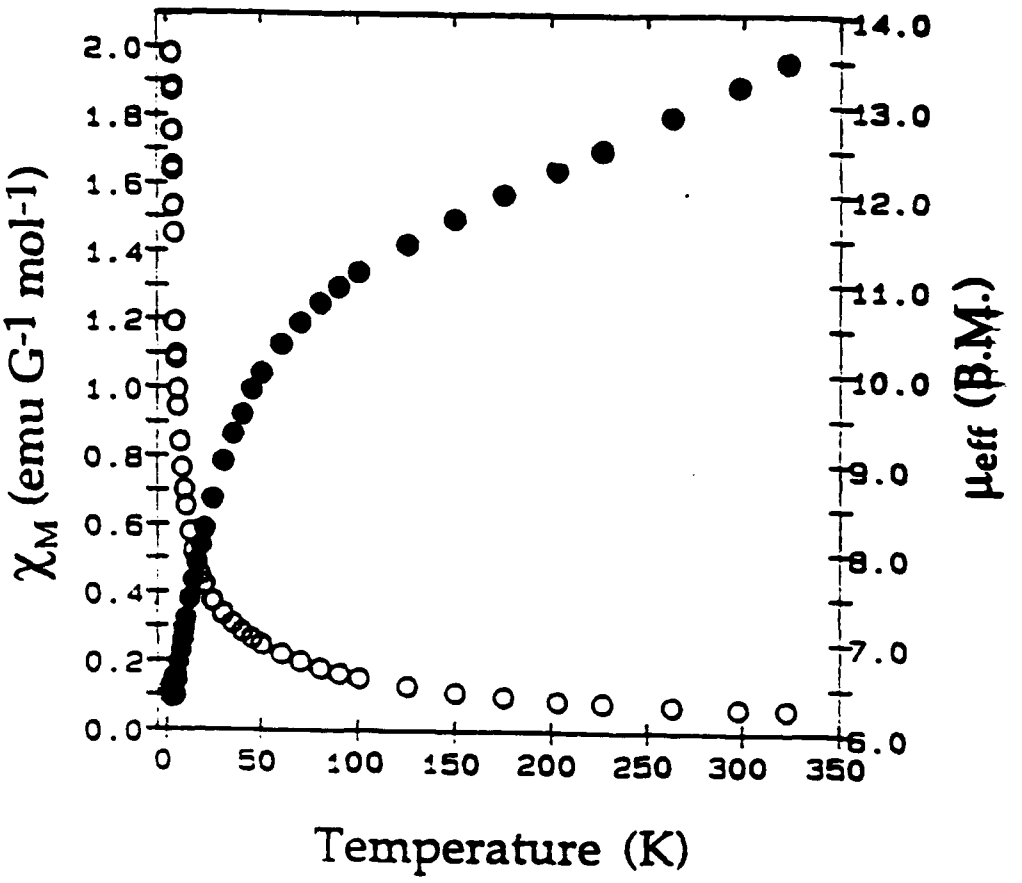

Fig. 19. Temperature-dependent molar susceptibility (o) and effective moment (•) plot for the [$Fe_{16}Mn$] cluster at 5 kG.

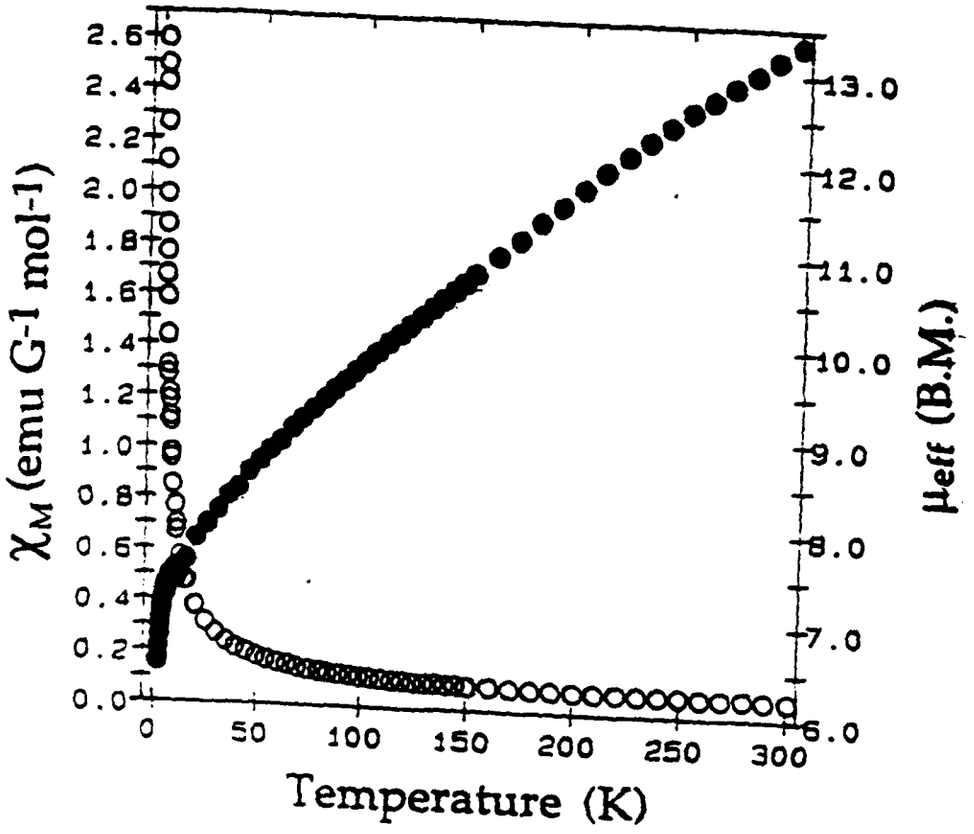

Fig. 20. Temperature-dependent molar susceptibility (o) and effective momen (•) plot for the [Fe_{17}] cluster at 5 kG.

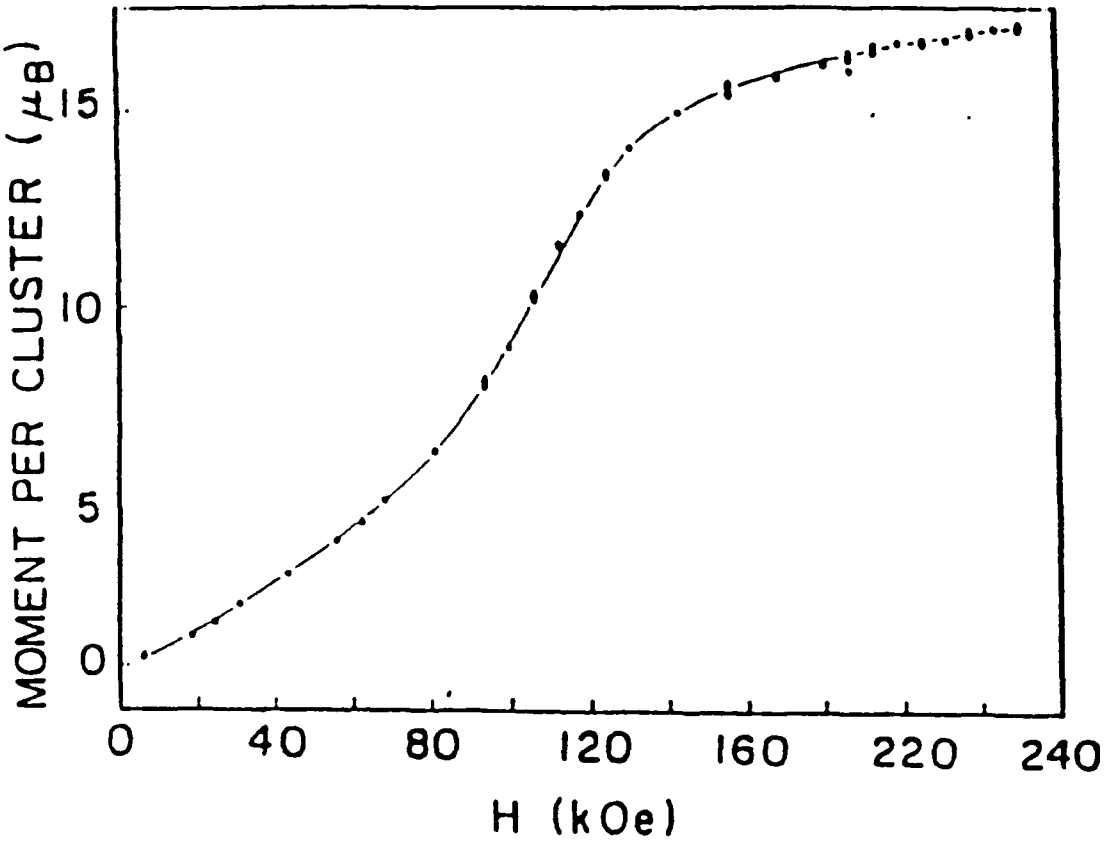

Fig. 21. High field magnetization study for [Fe_{11}] at 1.5 K.

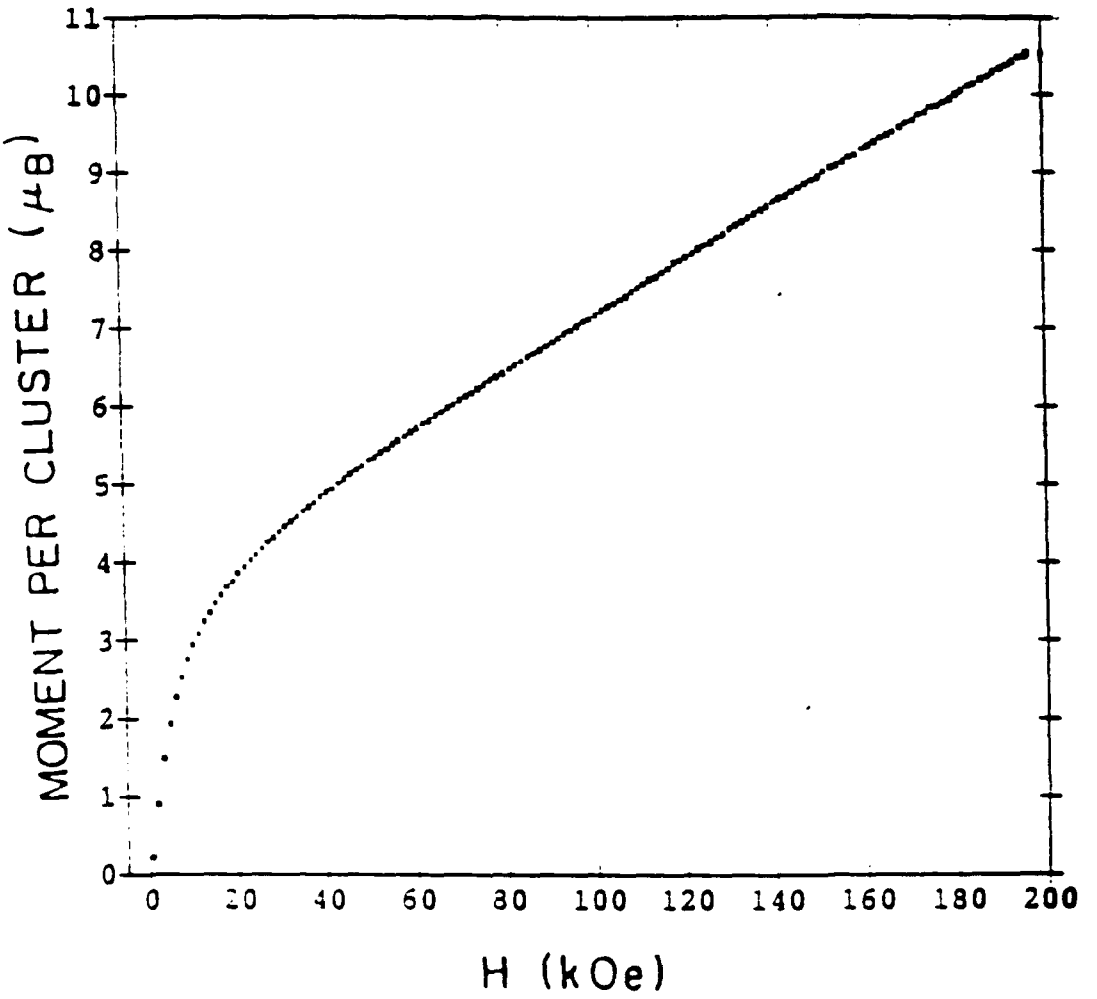

Fig. 22. Results of a high field magnetization study for [$Fe_{16}Mn$] at 1.48 K.

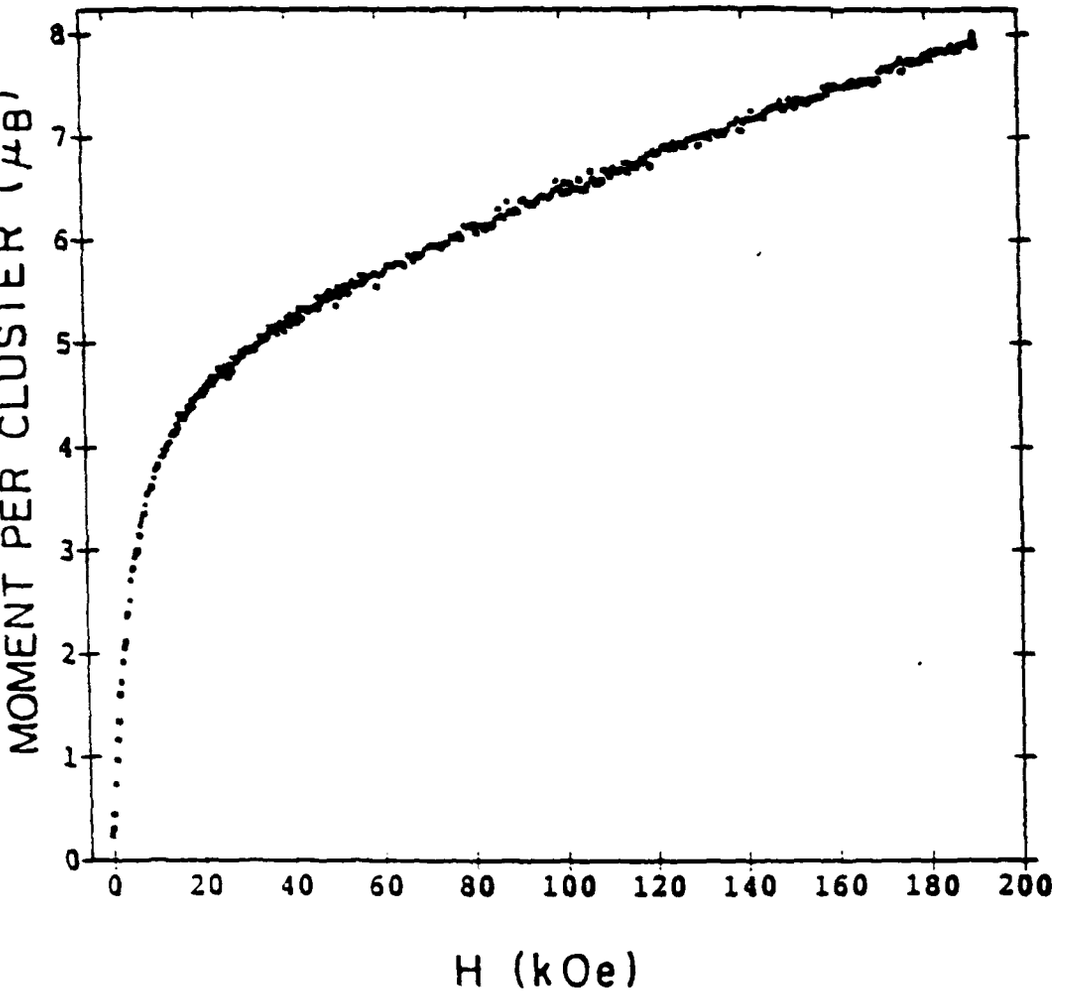

Fig. 23. Results of a high field magnetization study for [Fe_{17}] at 1.5 K.

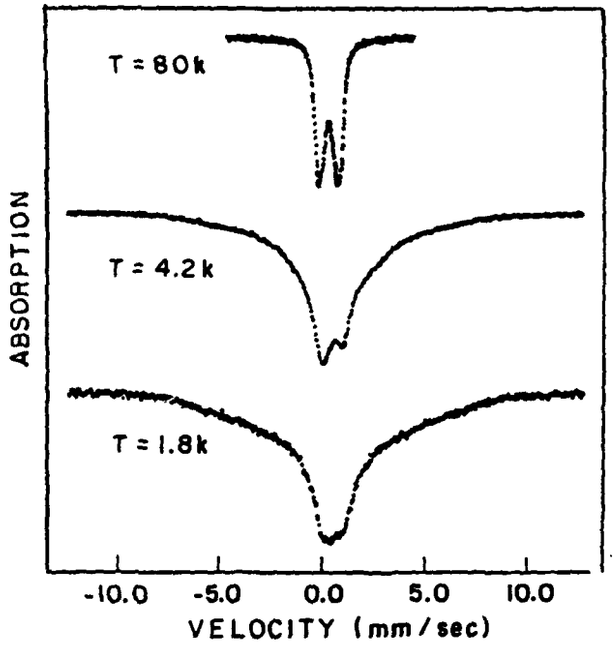

Fig. 24. Mössbauer spectra of polycrystalline $[Fe_{11}O_6(OH)_6(O_2CPh)_{15}].6THF$ at various temperatures.

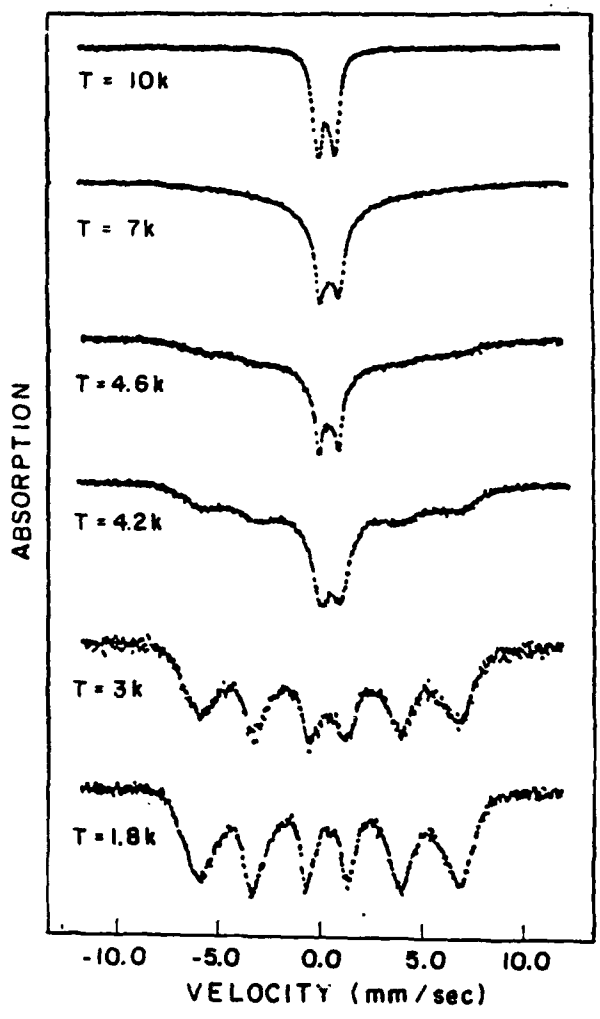

Fig. 25. Mössbauer spectra of polycrystalline $[Fe_{16}MnO_{10}(OH)_{10}(O_2CPh)_{20}]$ at various temperatures.

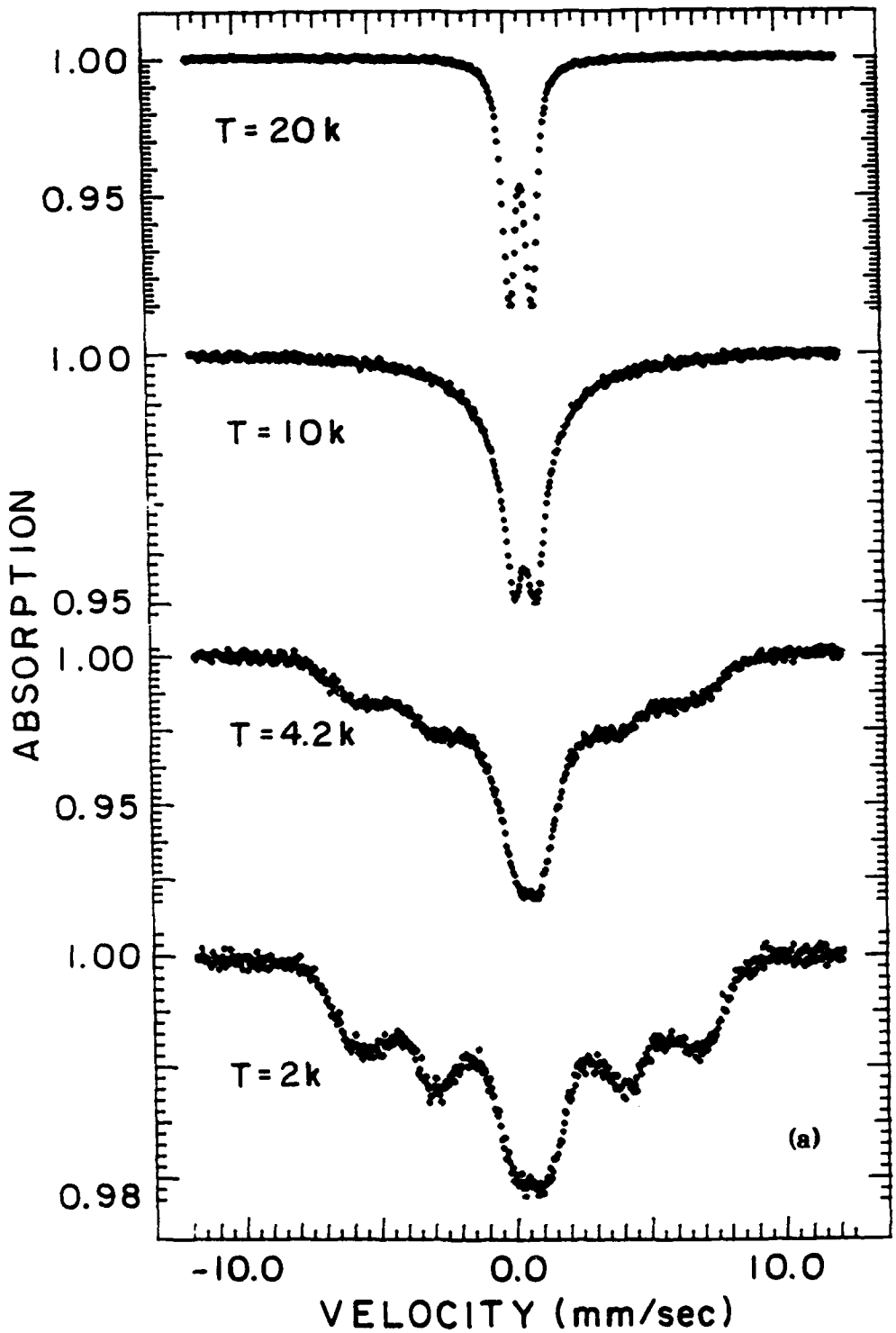

Fig. 26. Mössbauer spectra of polycrystalline $[Fe_{17}O_{10}(OH)_{10}O_2CPh)_{20}]$ at various temperatures.

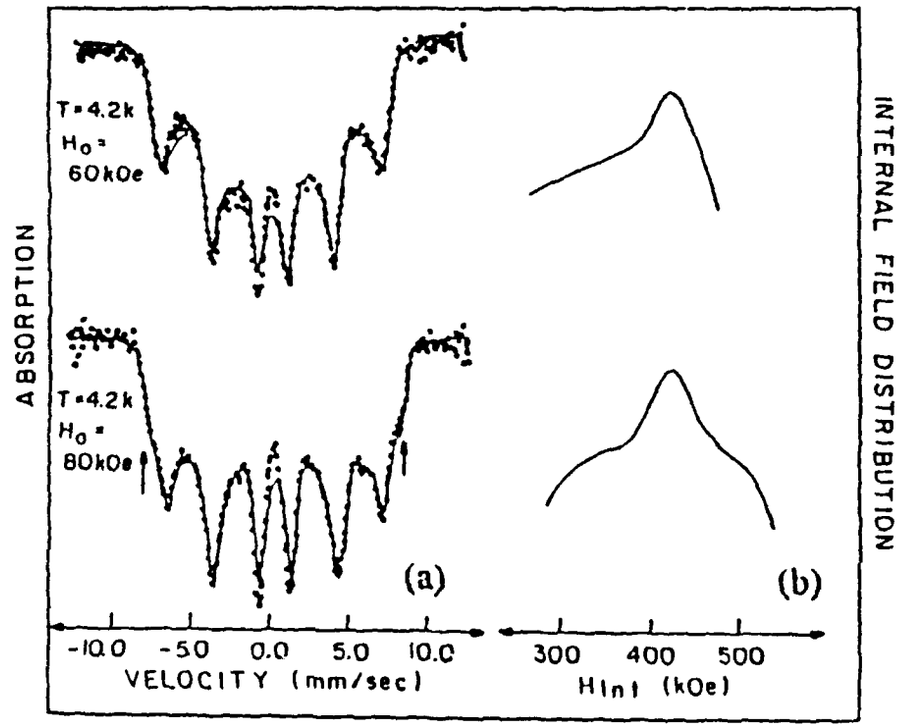

Fig. 27. (a) Low temperature Mössbauer spectra of 2 in external magnetic fields, H_0, parallel to the γ-ray direction. The solid line is a least-square fit of the experimental data to a distribution of internal magnetic fields. (b) The resulting distribution of internal magnetic fields at the sites of the iron nuclei.

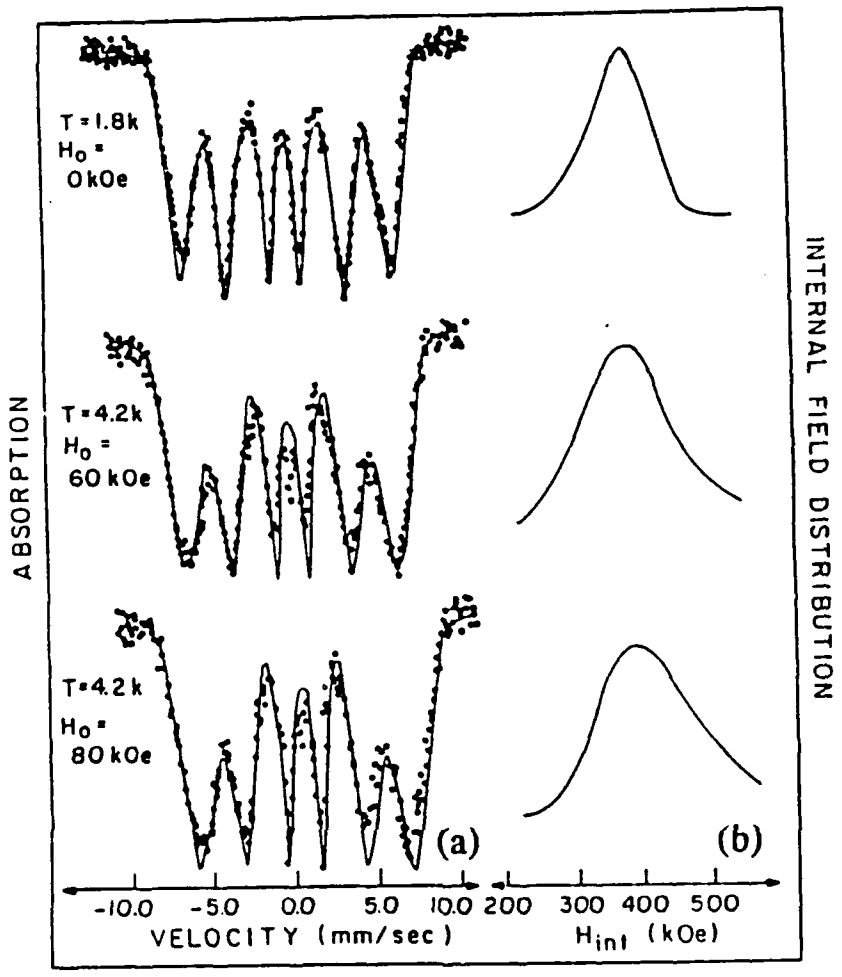

Fig. 28. (a) Low temperature Mössbauer spectra of 5 in the absence and presence of a longitudical external magnetic field, H_o. The solid line is a least-square fit of the experimental data to a distribution of internal magnetic fields. (b) The resulting distribution of internal magnetic fields at the sites of the iron nuclei.

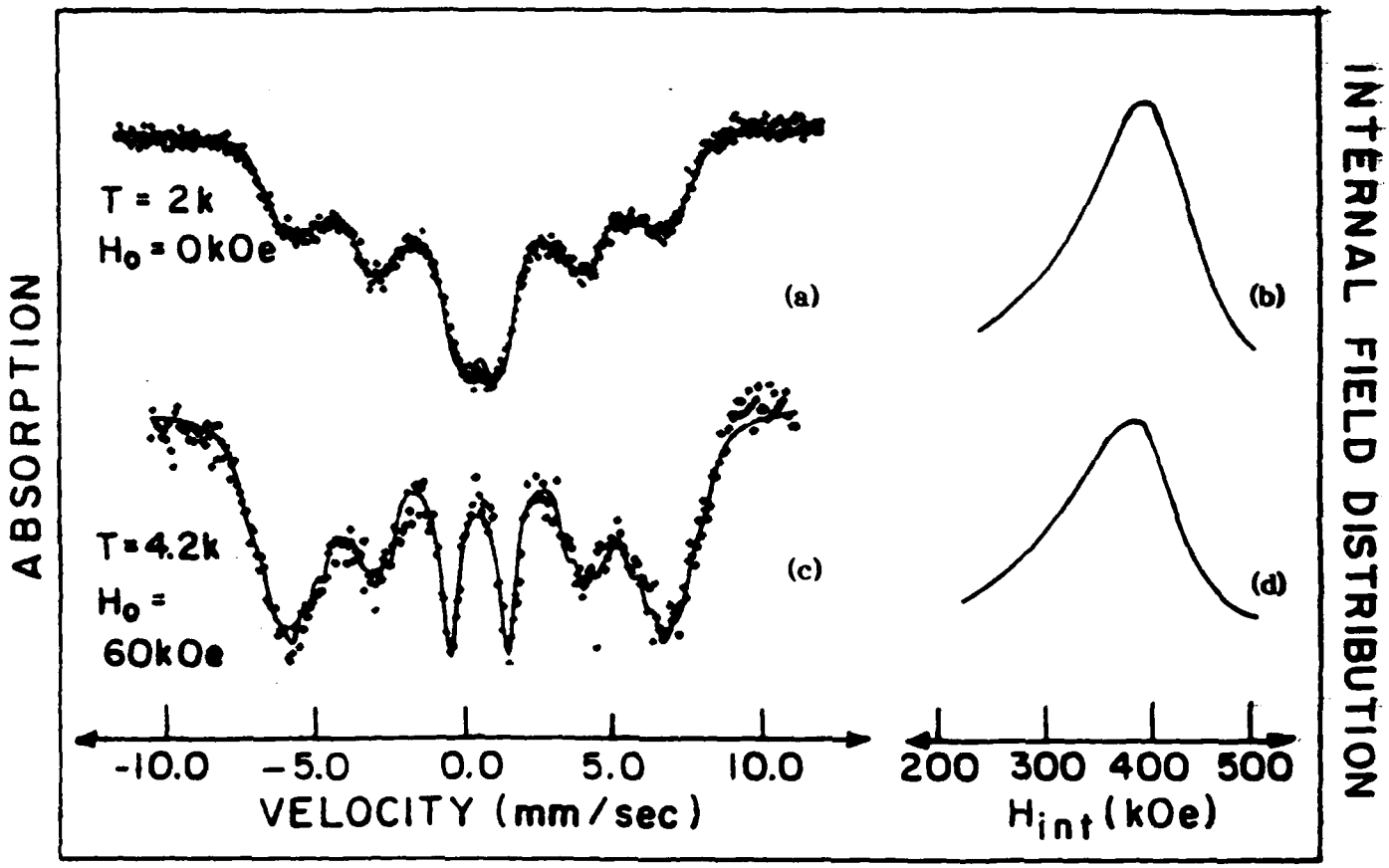

Fig. 29. (a) Low temperature Mössbauer spectra of 6 in the absence and presence of a longitudical external magnetic field, H_0. The solid line is a least-square fit of the experimental data to a distribution of internal magnetic fields. (b) The resulting distribution of internal magnetic fields at the sites of the iron nuclei.

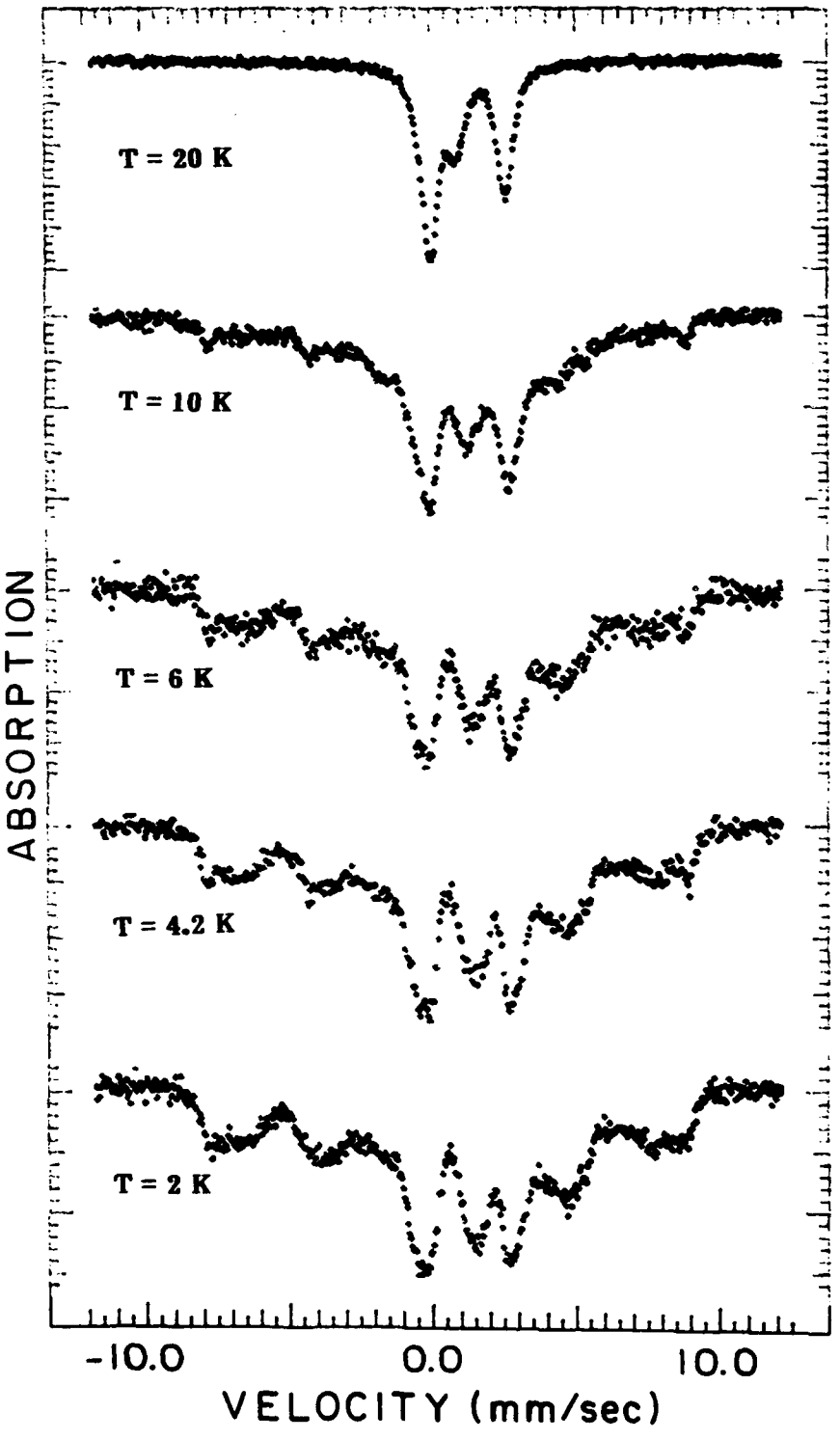

Fig. 30. Temperature-dependent Mössbauer spectra of $[Fe_{12}(O)_2(OCH_3)_{14}(O_2CCH_3)_{10}(CH_3OH)_2]$ Li_2 (3)

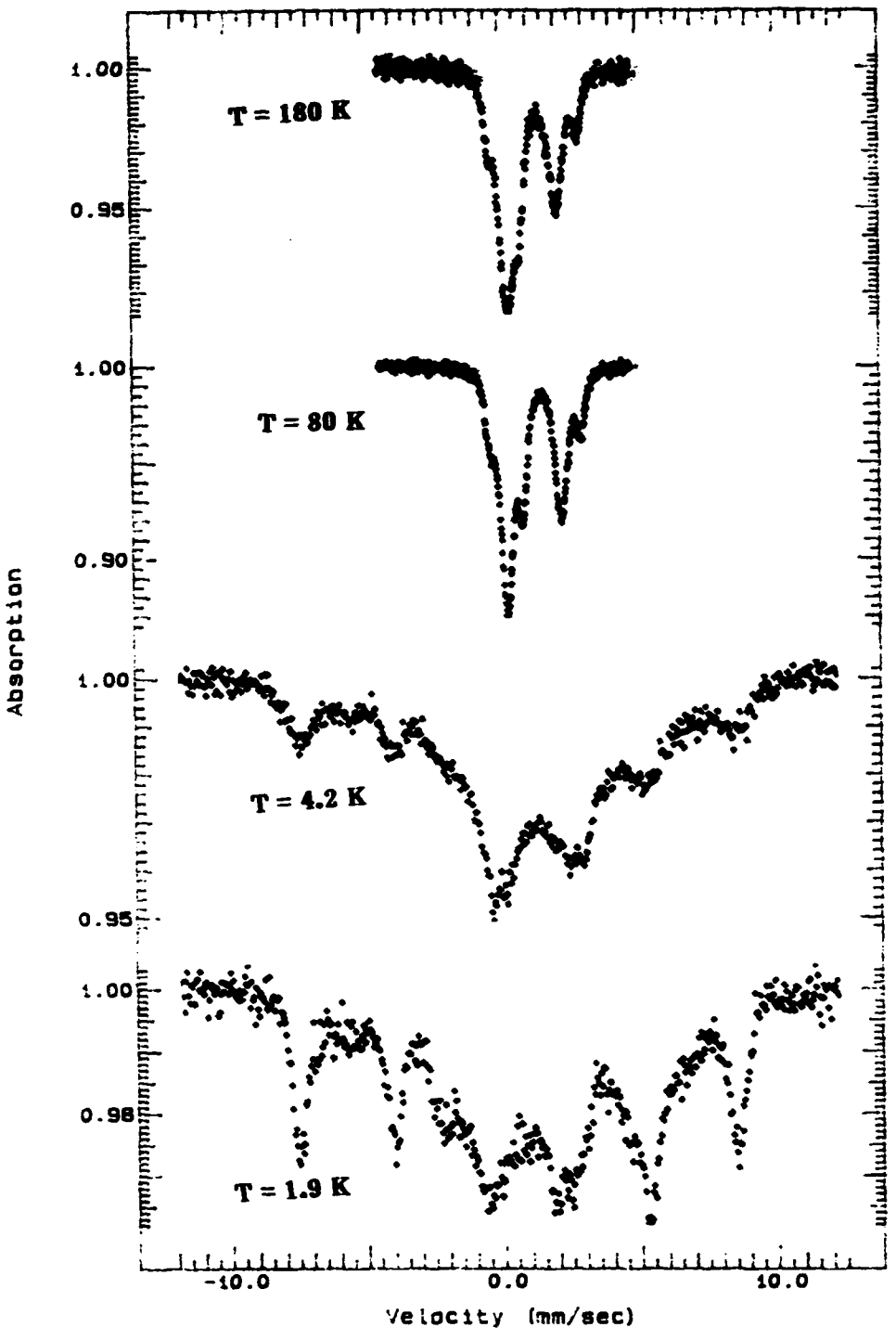

Fig. 31. Temperature-dependent Mössbauer spectra for $[Fe_{12}(O)_2(OCH_3)_{18}(O_2CCH_3)_6(CH_3OH)_4]$ (4).

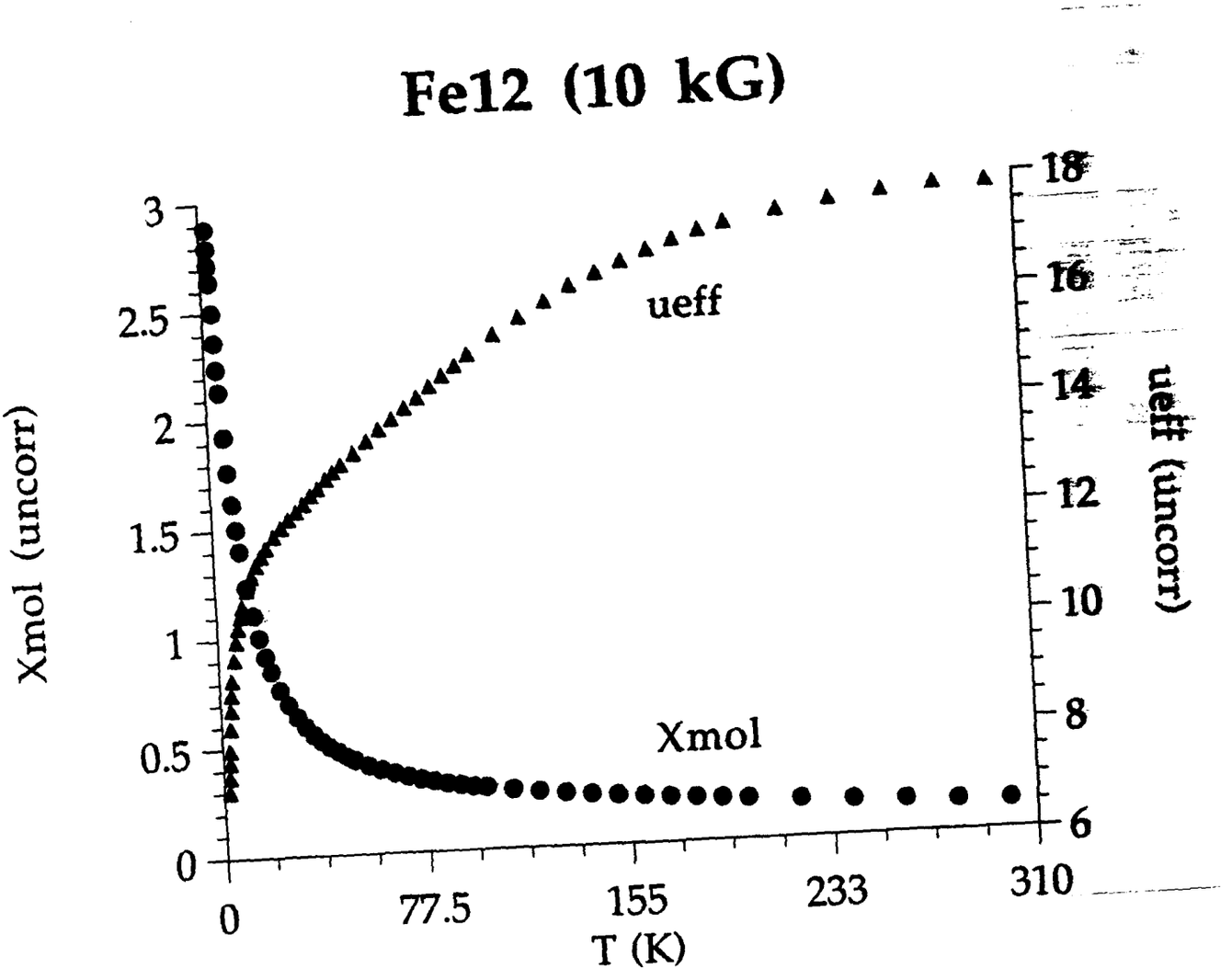

Fig. 32. Susceptibility studies for $[Fe_{12}(O)_2(OCH_3)_{18}(O_3CCH_3)_6(CH_3OH)_4]$ (4). Overall paramagnetic behavior is seen. The sharp increase of μ_{eff} with temperature indicates the presence of low-lying higher spin states.

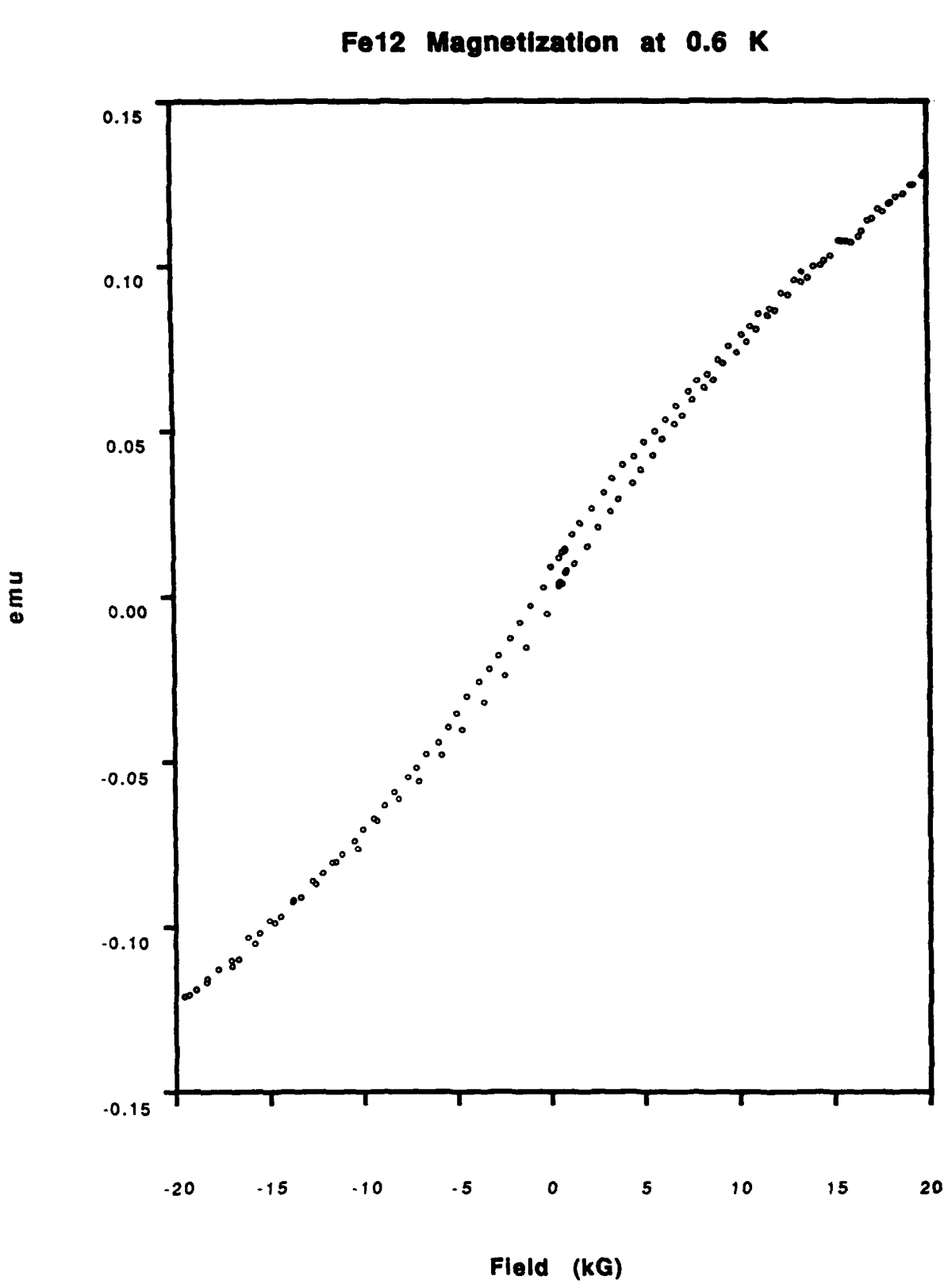

Fig. 33. Onset of hysteretic effects for compound 4 at low temperatures. The traces at 1.4 K and 0.6 K are indistinguishable.

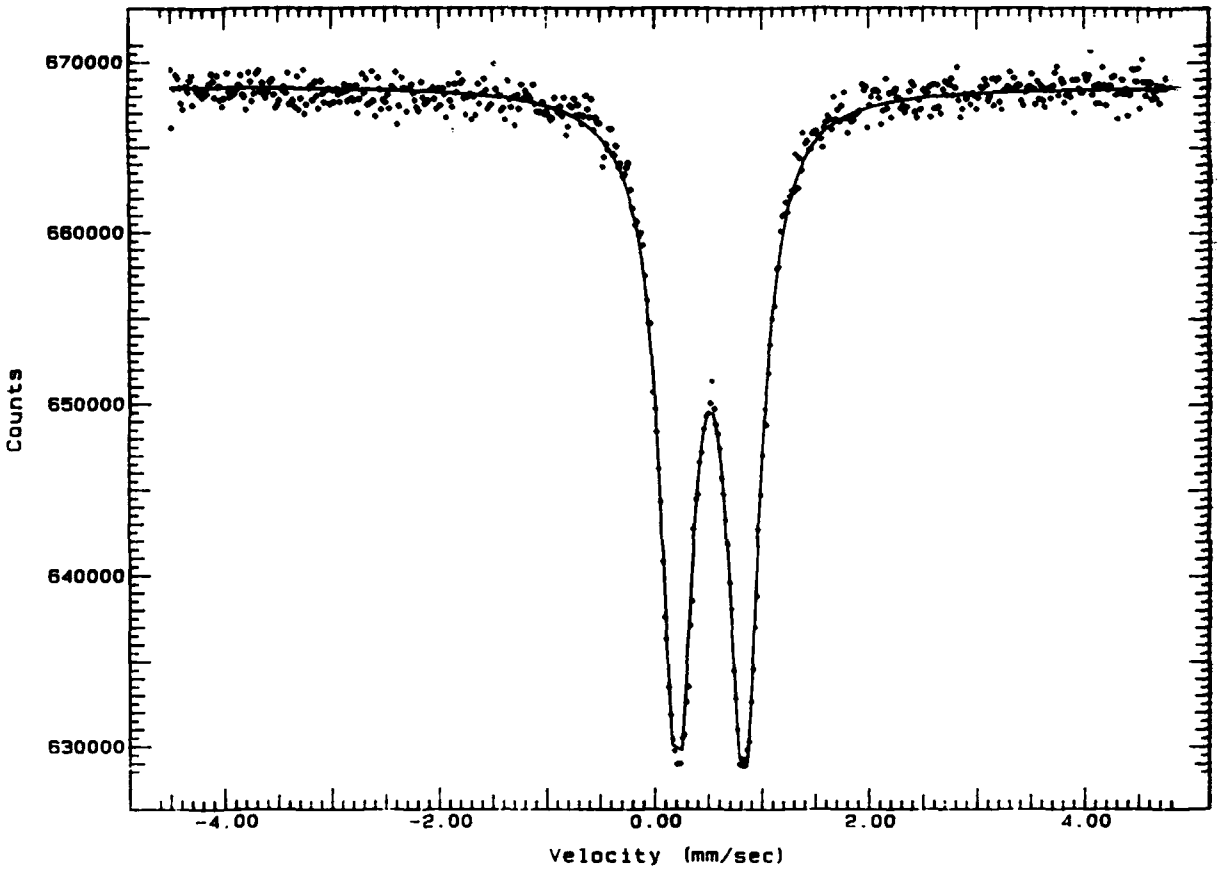

Fig. 34. Mössbauer spectra of the "ferric wheel" $[Fe(OCH_3)_2(O_2CCH_2Cl)]_{10}$(1) at 4.2 K.

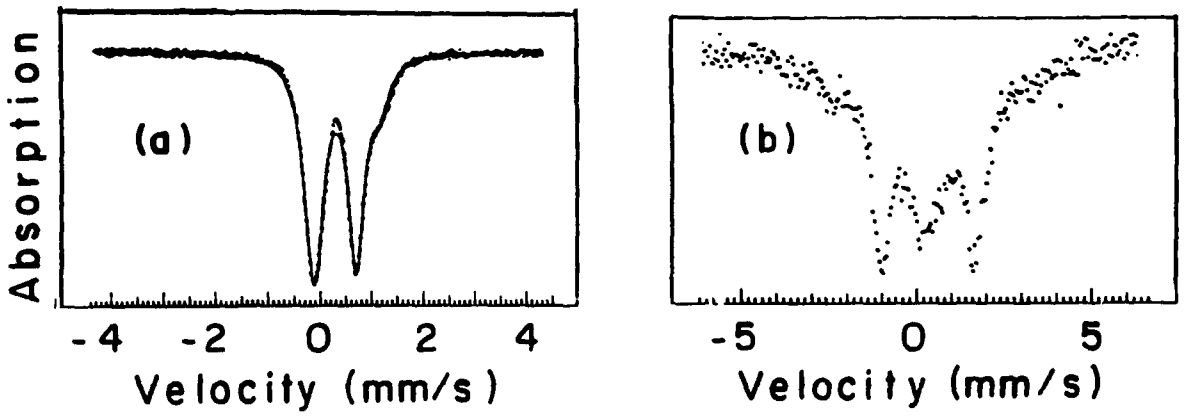

Fig. 35. (a) Mössbauer spectra of polycrystalline $(Pr_4N)_6Na_4Fe_{18}S_{30}\cdot 14$ MeCN at T = 4.2 K. The solid line is a least-square fit to the superposition of two quadrupole doublets (see text). (b) Mössbauer spectra of polycrystalline $(Bu_4N)_{4.5}Na_{13.5}Fe_{20}Se_{38}\cdot$ 2PhNH COMe·15EtOH at T = 4.2 K and H_0 = 80 KOe parallel to the γ-ray.

IX. APPENDIX

A. Lectures

The following is a list of lecture presentations by the P.I. at university or conference settings, on the subject supported by the contract.

1) **Iron Aggregation in Biological Systems: From Molecular Complexation to Biomineralization,** Francis Bitter National Magnet Laboratory, IAP Seminar Cambridge, MA (January 1990).

2) **"The Magnetochemistry of Supramolecular Particles: The Transition from the Molecular to the Solid-State,"** ONR contractors' meeting, Lake Arrowhead, CA (January, 1990)

3) **Nanometer-sized Structures and the Transition from the Molecular to the Solid-State,** Physics Seminar, Clark University, Worcester, MA (February 1990).

4) **Search for Collective Magnetic Correlations in Large Molecular Clusters,** Joint Japan-US Workshop on Novel Microcluster Assemblies, University of Maryland, College Park, Maryland (March, 1990).

5) **Ferritin: A Natural Laboratory for the Formation of Iron-mineral Nanophases** Seminar, Institute for Materials Science, Nuclear Research Center Demokritos, Athens, Greece (September, 1990).

6) **Observation of Collective Magnetic Correlations in Macromolecular Systems,** Physics Seminar, Emory University, Atlanta, GA (April, 1991).

7) **Molecular Clusters of 3D and Lower Magnetic Dimensionality,** MRS meeting Symposium on Clusters and Cluster-Assemblied Materials, Boston, MA (November, 1991).

B. Internal Reports

1) Contributions to the Francis Bitter National Magnet Laboratory Annual Reports to NSF (1990, 1991, 1992).
2) Contribution to the MIT Proposal to NSF for a National High Magnetic Field Laboratory (May, 1990).
3) Grant Applications to NSF (July, 1991), AFOSR (July, 1991) and NIH (February, 1992).

C. Collaborators

R.H. Holm, Professor of Chemistry, Harvard University

S.J. Lippard, Professor of Chemistry, MIT

D. Graduate Students Associated with the Project

At MIT S. Gorun, R.L. Rardin, W. Micklitz, V. McKee, K. Taft

At Harvard J.F. You, S.B. Yu, B. Snyder

E. List of Publications on iron clusters authored or coautored by the Principlal Investigator derived from support under the Grant.

1. G.C. Papaefthymiou
   Nanometer-sized Clusters and the Transition from the Molecular to the Solid-State.
   Submitted to *Phys.Rev. B.*

2. Georgia C. Papaefthymiou
   Observation of Collective Magnetic Correlations in Molecular Systems.
   To be submitted to the *J. Solid State Chem.*

3. G.C. Papaefthymiou
   "Supramolecular Particles: The Transition from the Molecular to the Solid State". In a Series onRadom Processes and Materials, *On Clusters and Clustering: From Atoms to Fractals,* Edited by P. Reynolds (North Holland), in press.

4. Jing-Feng You, G.C. Papaefthymiou, and R.H. Holm
   $[\beta\text{-}Na_2Fe_{18}S_{30}]^{8-}$ and $[Na_9Fe_{20}Se_{38}]^{9-}$: High Nuclearity Clusters by Mono- or Bicyclization of Unidimensional Polymeric Fragments and theExistence of Isomeric Monocyclic Clusters
   J. Am. Chem. Soc. **114,** 2697 (1992).

5. G.C. Papaefthymiou
   Molecular Clusters of 3D and Lower Magnetic Dimensionality in Clusters and Cluster-Assembled Materials, edited by R.S.Averback, J. Bernholc, and D.L. Nelson, MRS Symposium Proceedings, Vol. 206 (Materials Research Society, Pittsburgh, 1991), p.539.

6. Peter Poganiuch, Shuncheng Liu, Georgia C. Papaefthymiou, and Stephen J. Lippard
   A Trinuclear, Oxo-centered Mixed Valence Iron Complex with Unprecedented Carboxylate Coordination: $[Fe_3O(O_2CCH_3)_6(TACN)]\bullet 2CHCl_3$
   J. Am.. Chem. Soc. **113,** 4645 (1991)

7. B.S. Snyder, M.S.Reynolds, R.H. Holm, G.C. Papaefthymiou, and R.B.Frankel
   Electronic Properties of Monocapped Prismane and Basket Iron-Sulfur Clusters
   Polyhedron **10,**203 (1991).

8. Shi-bao Yu, G.C. Papaefthymiou, and R.H.Holm
   Comprehensive Iron-Selenium-Thiolate Cluster Chemistry
   Inorg. Chem. **30,** 3476 (1991).

9. Jing-Feng You, Barry S. Snyder, G.C. Papaefthymiou, and R.H.Holm
   On the Molecular/Solid State Boundary. A Cyclic Iron-Sulfur Cluster of Nuclearity Eighteen: Synthesis, Structure, and Properties
   J. Am. Chem. Soc. **112,** 1067 (1990).

10. J.-F. You, B.S. Snyder, R.H. Holm and G.C. Papaefthymiou

$[Na_2Fe_{18}S_{30}]^{8-}$, A High Nuclearity Cyclic Cluster Containing No Terminal Ligations: Amidate Supported Formation, Structural Diversity, Novel Physical Properties
J. Inorganic Biochemistry **36**(3-4), 175 (1989).

11. W. Micklitz, V. McKee, G.C. Papaefthymiou, R.L. Rardin, and S.J. Lippard
Models of Iron Nucleation in the Ferritins
In preparation.

12. R.B. Frankel, G.C. Papaefthymiou, and G.D. Watt
Variation of Superparamagnetic Properties with Iron Loading of Mammalian Ferritin
Hyperfine Interactions **66,** 71 (1991).

13. S. Ciurli, M.Carrié, J.A. Weigel, M.J. Carney, T.D.P. Stack, G.C. Papaefthymiou, and R.H.Holm
Subsite-Differentiated Analogues of Native $[4Fe\text{-}4S]^{2+}$ Clusters: Preparation of Clusters with Five- and Six-Coordinate Subsites and Modulation of Redox Potentials and Charge Distributions
J. Am. Chem. Soc. **112,** 2654 (1990).

14. R.B. Frankel, G.D. Watt and G.C. Papaefthymiou
Mössbauer Spectroscopy of Fe^{2+} Binding to Apo and Holo Mammalian Ferritin, In *Applications of the Mössbauer Effect,* Edited by E. Baggio-saitovitch, E. Galvãoda Silva, and R.H. Rechenberg (World Scientific, London 1990), p.160.